JBC Papers in Press. Published on October 31, 2007 as Manuscript M706399200
The latest version is at http://www.jbc.org/cgi/doi/10.1074/jbc.M706399200

The Interactions of Cell Division Protein FtsZ with Guanine Nucleotides

Sonia Huecas[1,*], Claudia Schaffner-Barbero[1], Wanius García[1,3], Hugo Yébenes[1,4], Juan Manuel Palacios[1,5], José Fernando Díaz[1], Margarita Menéndez[2], and José Manuel Andreu[1,*]

From [1]Centro de Investigaciones Biológicas, CSIC, Madrid, Spain, and [2]Instituto de Química-Física Rocasolano, CSIC, Madrid, Spain.

Running head: FtsZ-nucleotide interactions and polymer dynamics

*To whom correspondence should be addressed: Centro de Investigaciones Biológicas, CSIC, Ramiro de Maeztu, 9, 28040 Madrid, Spain. E-mail: j.m.andreu@cib.csic.es; sonia@cib.csic.es. Tel: +34 918373112, ext 4381. Fax: +34 915360432.
[3]Current address: Centro de Biotecnologia Molecular e Estrutural, Instituto de Física de São Carlos, USP, Brazil. [4]Current address: Centro Nacional de Biotecnología, CSIC, Madrid, Spain. [5]Current address: GlaxoSmithKline, Madrid, Spain

Prokaryotic cell division protein FtsZ, an assembling GTPase, directs the formation of the septosome between daughter cells. FtsZ is an attractive target for the development of new antibiotics. Assembly dynamics of FtsZ is regulated by the binding, hydrolysis and exchange of GTP. We have determined the energetics of nucleotide binding to model apo-FtsZ from *Methanococcus jannaschii* and studied the kinetics of mant-nucleotide binding and dissociation from FtsZ polymers, employing calorimetric, fluorescence and stopped-flow methods. FtsZ binds GTP and GDP with K_b values ranging from 20 to 300 μM^{-1} under various conditions. GTP·Mg^{2+} and GDP·Mg^{2+} bind with slightly reduced affinity. Bound GTP and the coordinated Mg^{2+} ion play a minor structural role in FtsZ monomers, but Mg^{2+}-assisted GTP hydrolysis triggers polymer disassembly. Mant-GTP binds and dissociates quickly from FtsZ monomers, with ~10-fold lower affinity than GTP. Mant-GTP displacement measured by fluorescence anisotropy provides a method to test the binding of any competing molecules to the FtsZ nucleotide site. Mant-GTP is very slowly hydrolyzed and remains exchangeable in FtsZ polymers, but it becomes kinetically stabilized, with a 30-fold slower k_+ and ~500-fold slower k- than in monomers. The Mant-GTP dissociation rate from FtsZ polymers is comparable to the GTP hydrolysis turnover and to the reported subunit turnover in *Escherichia coli* FtsZ polymers. Although FtsZ polymers can exchange nucleotide, unlike its eukaryotic structural homologue tubulin, GDP dissociation may be slow enough for polymer disassembly to take place first, resulting in FtsZ polymers cycling with GTP hydrolysis similarly to microtubules.

FtsZ is a cytoskeletal protein essential to bacterial cytokinesis and a member of the tubulin family of GTPases, which also includes αβ-tubulin (1), γ-tubulin (2), bacterial tubulin BtubA/B (3,4) and TubZ (5). FtsZ assembles by forming filaments that constitute the Z-ring at the cell division site in bacteria. The Z-ring, a dynamic structure maintained by assembly and disassembly of FtsZ, recruits the other elements of the division machinery following chromosome segregation (6-10). Bacterial cell growth and division are regulated by nutrient availability: a metabolic sensor has been recently identified in *Bacillus subtilis*, including an effector, the glucosyltransferase UgtP, which modulates FtsZ assembly (11). GTP binding, hydrolysis and exchange constitute the regulatory mechanism responsible for dynamics of FtsZ and tubulin polymers. The nucleotide switches of these assembling GTPases appear to involve polymerization-driven structural changes (12), although FtsZ and tubulin form different end polymers. The GTPase activity of FtsZ is modified by the polymerization inhibitory protein MipZ (13) and, weakly, by EzrA (14).

The hydrolysable nucleotide bound to tubulin becomes occluded in microtubule protofilaments (15). Microtubules hydrolyze all bound GTP to GDP except at their very ends and become metastable, giving rise to microtubule

dynamic instability (16). In contrast, polymers of FtsZ from *E. coli* were reported to contain mostly GTP and, under certain conditions, nucleotide exchange proceeds faster than hydrolysis (17). This suggested that the nucleotide binding site remains exchangeable in FtsZ polymers, which would therefore be devoid of dynamic instability. Polymers of *M. jannaschii* FtsZ were found to contain different proportions of GTP and GDP (depending on the hydrolysis rate) and to rapidly depolymerize upon either GTP consumption or GDP addition (18,19). GDP binding destabilizes *M. jannaschhi* FtsZ polymers compared to polymers with GTP or without a bound nucleotide (20). In *E. coli* FtsZ polymers the main rate-limiting step in nucleotide turnover was found to be nucleotide hydrolysis, rapidly followed by phosphate release, while a second rate-limiting step could be nucleotide dissociation. However, whether nucleotide dissociation took place directly from the polymer or through depolymerization into subunits, followed by GDP release, was not determined (21).

An important problem yet to be solved for FtsZ assembly dynamics is whether, following GTP hydrolysis, i) GDP dissociates from subunits in the FtsZ polymer which directly reload with GTP, or ii) polymer subunits exchange with GTP-bound subunits in solution, or iii) the FtsZ-GDP polymer fully disassembles and reassembles again from GTP-bound subunits. Consistent with an exchangeable nucleotide in FtsZ polymers, the nucleotide was observed to be largely accessible in the crystal structure of a protofilament-like dimer of *M. jannaschii* FtsZ (22). On the other hand, exchange of GFP-FtsZ fusions in bacterial Z-rings was found to proceed with a half-time of 8-9 second *in vivo*, by means of fluorescence recovery after photobleaching (FRAP) (23,24). As observed in an *in vitro* fluorescence resonance energy transfer (FRET) assay, subunit turnover in filaments of *E. coli* FtsZ took place with a half-time of 7 seconds with GTP, which was slowed down under conditions reducing the nucleotide hydrolysis rate (25). This rate of subunit turnover is comparable to the turnover rate of GTP hydrolysis (21) and to the rate of depolymerization in GDP excess, suggesting that GDP does not exchange into intact filaments (23). This favors the interpretation that the rapid assembly dynamics of FtsZ filaments may operate by a mechanism related to microtubule dynamic instability (25). In addition, subunit turnover and GTPase in FtsZ from *Mycobacterium tuberculosis* are both about ten times slower than in *E. coli* FtsZ (26).

FtsZ and its nucleotide binding site are attractive targets for cell division inhibitors, which may lead to new classes of antibacterial compounds (27) to fight the continuous emergence of antibiotic resistance. Small molecules reported to modulate FtsZ assembly include 8-Br-GTP (28) and other nucleotide analogues (29), 3-metoxybenzamide (30), viriditoxin (31), ruthenium red (32), zantrins (33), SRI-3072 (34), polyphenols (35), PC58538 and PC170942 (36), sanguinarine (37), certain taxanes (38), A189 (39), amikacin (40), totarol (41) and cinnamalehyde (42).

This study focused on fundamental processes of FtsZ-nucleotide interactions. We have determined the energetics of GTP and GDP binding to FtsZ and the kinetics of binding and dissociation in FtsZ monomers and polymers using fluorescent mant-nucleotides. The results reveal functional differences with nucleotide binding to tubulin that will facilitate screening for compounds binding to the nucleotide site of FtsZ. They also indicate an slowed-down nucleotide exchange in FtsZ polymers, which provides insight to their dynamics.

EXPERIMENTAL PROCEDURES

Nucleotides- GDP was obtained from Sigma and GTP (lithium salt) from Roche Molecular Biochemicals or Sigma. 2'/3'-O-(N-methyl-anthraniloyl)-guanosine-5'-triphosphate and -diphosphate (mant-GTP and mant-GDP respectively) were from Jena Bioscience. [8-^{3}H]GTP (6 Ci/mmol) and α-^{32}P-GTP (~400 Ci/mmol) were from Amersham Biosciences. Nucleotides were analyzed (after extraction with perchloric acid in the case of protein samples; (18) by HPLC with a Grace Vydac 3021c4.6 anion exchange column (0.46 x 25 cm) eluted with a linear gradient of 25 mM NaH_2PO_4/Na_2HPO_4, pH 2.8, to 125 mM NaH_2PO_4/Na_2HPO_4, pH 2.9. All other chemicals (analytical grade) used were from Merck or Sigma.

Preparation of nucleotide-free FtsZ from M. jannaschii- FtsZ (without histidine tag) was overproduced in *E. coli* BL21(DE3)pLys and was purified as described (18,19). Nucleotide-free FtsZ (apo-FtsZ) was prepared as described (20) with minor modifications. FtsZ was incubated in 2.5 M guanidinium chloride

(GdmCl) for 30 min at room temperature, followed by gel filtration in a 0.9 x 25 cm Sephadex G-25 column in 25 mM Pipes/KOH, and 2.5 M GdmCl, pH 7.5, to separate the released nucleotide from protein (monitored spectrophotometrically at 254 and 280 nm). A second G-25 column in 25 mM Pipes/KOH, 50 mM KCl, and 1 mM EDTA, pH 7.5 (Pipes-KCl buffer) was used to eliminate GdmCl and equilibrate the protein in this experimental buffer. Apo-FtsZ concentration was measured spectrophotometrically employing an extinction coefficient ε_{280} = 6990 M^{-1} cm^{-1} (calculated for 1 Trp, 1 Tyr). Apo-FtsZ was frozen and stored in liquid nitrogen and was melted on ice before use.

Differential Scanning Calorimetry (DSC)- Measurements were performed using a VP-DSC microcalorimeter (Microcal, Inc.). Samples were degassed at room temperature prior to calorimetric experiments. Calorimetric cells (operative volume ~ 0.5 ml) were kept under an extra constant pressure of 2 atm to prevent degassing during the scan. Standard VP-Viewer and Origin-DSC software (MicroCal, Inc.) were used for data acquisition and analysis. Excess heat capacity (C_p) was obtained after subtraction of the buffer-buffer baseline, and the denaturation enthalpy (ΔH_D) was determined from the area under the absorption peak. Measurements were performed at a scan rate of 30 ºC/h in Pipes-KCl buffer using 12 µM FtsZ. GXP, and Mg^{2+} concentrations were 100 µM and 10 mM, respectively.

Isothermal titration calorimetry (ITC)- Calorimetric titrations of FtsZ with GXP, GXP-Mg and Mg^{2+} were performed at 25 ºC using a MCS titration calorimeter (MicroCal, Inc). Measurements were carried out in Pipes-KCl buffer, supplemented with 10 mM Mg^{2+} in both protein and nucleotide solutions for titration experiments with GXP·Mg^{2+} (EDTA was omitted for titration with Mg^{2+}). Samples were dialyzed against buffer before measurements. Ligand solutions (~150 µM GXP or 50 mM Mg^{2+}) were prepared in the dialysis buffer. FtsZ (10 to 25 µM) solution was loaded into the calorimeter cell and titrated, typically, by adding 1 x 1µl, plus 16 to 22 injections (10-12 µl), of a concentrated solution of the ligand. Heats of titrant dilution were determined in separate runs and subtracted, when required, to obtain the heat of binding. Binding isotherms were analyzed by nonlinear regression analysis to a single-set of sites model, using software supplied by the manufacturer, to calculate the number of binding sites (n), the binding constant (K_b) and the enthalpy of binding (ΔH).

Stoichiometry of binding of nucleotides and apo-FtsZ polymerization- The stoichiometry of binding of GTP, GDP, mant-GTP and mant-GDP to soluble apo-FtsZ was measured using a centrifugation assay. Apo-FtsZ (6 or 8 µM) was incubated at 25ºC for 30 min with nucleotides at different known concentrations (3-15 µM) in a final volume of 0.6 mL Pipes-KCl buffer. Samples were then centrifuged for 2.5 h at 100.000 rpm and 25ºC in a TLA-120.2 rotor employing a Beckman Optima TLX ultracentrifuge. After centrifugation, the top 0.3 mL were carefully withdrawn and the concentration of free nucleotide was determined spectrophotometrically employing the extinction coefficients ε_{254} = 23300 M^{-1} cm^{-1} for mant-nucleotides and ε_{254} = 13620 M^{-1} cm^{-1} for GTP and GDP. The top half contained only free nucleotide and essentially no protein, as checked by control measurements, and the bottom half all the protein, in chemical equilibrium with free nucleotide. The nucleotide bound to FtsZ was calculated as the difference of the the known total concentration of nucleotide minus the free concentration in the top part of the solution.

To measure the stoichiometry of binding of mant-GTP to apo-FtsZ polymers, 20 µM apo-FtsZ was polymerized at 55ºC in Pipes-KCl Buffer with 10 mM $MgCl_2$. After 10 min, 20 µM mant-GTP was added. After 1, 10 and 20 min, different aliquots of 0.1 mL were taken and centrifuged for 6 min at 80.000 rpm in a prewarmed TLA-100 rotor employing a Beckman Optima TLX ultracentrifuge (18). After centrifugation, the supernatant was carefully withdrawn and the pellet was resuspended in buffer. FtsZ concentration was measured in the supernatant and in the pellet with the Bio-Rad protein assay kit (43) in multiwell plates, employing spectrophotometrically calibrated FtsZ standards and a Titertek Multiskan MC plate reader with a 595-nm filter. Mant-GTP bound to FtsZ was fluorometrically determined in the resuspended pellet employing a Shimadzu RF-540 spectrofluorometer (excitation wavelength 357 nm, emission wavelength 445, 5 nm excitation and emission slits) using standards of FtsZ-bound mant-GTP.

Affinity of binding of ^{3}H-GTP to apo-FtsZ- Binding of [8-^{3}H]-GTP to apo-FtsZ was measured by protein depletion (44) as follows.

Varying [8-^{3}H]-GTP concentrations were added to aliquots of apo-FtsZ (500 nM) in Pipes-KCl buffer (0.2 ml). Mixtures were centrifuged for 1.5 h, at 100,000 rpm and 25ºC in a Beckman TLA-100 rotor. The total [8-^{3}H]-GTP concentration was determined in the bottom half and the free concentration in the protein-depleted top half of tubes, after dilution in 1.5 mL Beckman ReadySafe, employing a Wallac Trilux 1450 Microbeta liquid scintillation counter (Perkin Elmer). In each assay, controls with [8-^{3}H]-GTP alone were included and concentrations corrected for the small amount of nucleotide sedimented in the absence of protein. When we measured the binding of [8-^{3}H]-GTP to an excess of apo-FtsZ, 1.8% of inactive ligand was found in the stock solution. This percentage was subtracted from the concentration of free [8-^{3}H]-GTP calculated in each assay.

Affinity of binding of mant-nucleotides to apo-FtsZ- Binding of mant-nucleotides to FtsZ was measured by the increase in fluorescence intensity and anisotropy of the probe. It was first confirmed that more than 95% of mant-GXP co-sedimented with an excess of apo-FtsZ upon high speed centrifugation. Fluorescence of free and FtsZ-bound mant-GXP was measured with a Fluorolog 3-221 instrument (Jobin Yvon-Spex, Longiumeau, France) employing an excitation wavelength of 357 nm and an emission wavelength of 445 nm, with 3 nm and 5 nm bandwidths respectively and 2 x 10 mm cells. Anisotropy was measured in T-format with 5 nm excitation bandwidth and 10 nm emission bandwidths. Protein-fluorescent ligand interaction was determined as reported (45), with modifications. Fixed concentrations of mant-GXP (10 - 500 nM) were first titrated with different apo-FtsZ concentrations (0 – 6 µM) in Pipes-KCl buffer, with or without 10 mM Mg^{2+}, to obtain the anisotropy increment, Δr_{max}, corresponding to all the mant-GTP bound. To do this, the increase in anisotropy was plotted against apo-FtsZ concentration and iteratively least-squares fitted with an isotherm of binding to one site. The estimated values of Δr_{max} were used to approximate the free apo-FtsZ concentrations and these new values were employed again, until an unchanging Δr_{max} value was obtained. The convergent data was used to calculate the binding constant of apoFtsZ to mant-GXP. Titration of ApoFtsZ (500 nM) with different mant-GTP concentrations was also measured and the data were model-fitted (empoying the Δr_{max} value) to yield the number of binding sites and the equilibrium binding constant of mant-GTP to apo-FtsZ.

Affinity of ligands competing with mant-GTP Competition assays were performed by measuring, through the decrease in fluorescence anisotropy, the displacement of mant-GTP from FtsZ. Different concentrations of competing ligand were mixed with apoFtsZ (500 nM) and mant-GTP (500 nM) in Pipes-KCl-10 mM $MgCl_2$ buffer (final volume of 0.4 ml) and the anisotropy measured at 25 ºC. The fraction of the reference ligand mant-GTP bound was plotted against the competing ligand concentration and data were fitted assuming that the two ligands bind to the same site. The resulting system of equations (45) was numerically solved with the program Equigra v 5.0 (46) or with a MATLAB script (unpublished; available upon request), which provided the best-fitted value of the equilibrium binding constant of the competing ligand.

The relative affinity of FtsZ for GDP and GTP was directly determined by incubating apo-FtsZ with solutions of different ratios of GTP/GDP for 1 h at 25 ºC in 50 mM Tris-HCl, 50 mM KCl, 1 mM EDTA, pH 7.5 (Tris-KCl buffer). Excess nucleotide was removed by a chromatography in a fast desalting column HR 10/10 (Amersham Biosciences) equilibrated in the same buffer with 10 µM nucleotide at the same GDP/GTP ratio. Eluted protein was precipitated with perchloric acid and nucleotide content was measured by HPLC.

Kinetics of binding and dissociation of mant-nucleotides to apo-FtsZ- Kinetic measurements were made with a Bio-Logic SFM-400 T-format stopped-flow device equipped with a fluorescence detection system. A wavelength of 368 nm in the excitation pathway and a filter with a cut-off of 450 nm in the emission pathway was employed. When measuring light scattering at the same time, a 350 nm band-pass filter was included in the second emission pathway. Five to ten separate curves were averaged for each condition and the curves so obtained were fitted to a single-, double- or triple-exponential equation of the form $y(t) = at + b + \sum A_i e^{-ki\ t}$ (where the slope (a) and offset (b) correspond to the linear drift after the reaction). The best-fitting rate constants, k_i, and amplitudes, A_i, were determined with the Bio-Kine software (Bio-Logic) or with a nonlinear least squares fitting program based on the Marquardt algorithm (47).

Histidine-tagged FtsZ polymers- FtsZ-His_6 and mutant FtsZ-W319Y-His_6 were overproduced in *E. coli* and affinity purified as described (19). Apo-FtsZ-W319Y-His_6 was prepared as apo-FtsZ above and its concentration measured with an extinction coefficient ε_{280} = 2980 M^{-1} cm^{-1} (2 Tyr). It was diluted at 55 °C into Pipes-KCl buffer, pH 6.5, supplemented with 6 mM $MgCl_2$ and nucleotides (the His tagged protein has a tendency to precipitate at pH < 7 at room temperature). FtsZ polymers were negatively stained and observed under a Jeol 1230 electron microscope.

Copolymers of FtsZ-W319Y-His_6 and FtsZ-His_6, formed in 50 mM Mes, 50 mM KCl, 1mM EDTA, pH 6.5 (Mes-KCl buffer) with 6 mM $MgCl_2$ and 0.1 mM GTP at 55 °C, were pelleted by centrifugation at 60,000 rpm, 6 minutes, at 55 °C in a prewarmed TLA-100 rotor. They were resuspended in 1% SDS and the concentration of the FtsZ-His_6 single Trp was measured fluorometrically by excitation at 295 nm, employing FtsZ-His_6 standards. Concentration of FtsZ-W319Y-His_6 polymers was measured with the Bio-Rad assay (43) with FtsZ-W319Y-His_6 standards. Exchange of α-^{32}P-GTP into FtsZ-W319Y-His6 or FtsZ-His_6, in Mes-KCl buffer with 6 mM $MgCl_2$ and 1 mM GTP at 55 °C, was measured employing a nitrocellulose filtration assay (17).

RESULTS

Effects of nucleotide on FtsZ secondary structure and thermal stability - Prior to studying the interactions of FtsZ with nucleotides, effects of the bound nucleotide on FtsZ stability were evaluated. The circular dichroism spectrum of stable nucleotide-free FtsZ from *M. jannaschii* (20) was not significantly different from that of FtsZ. The reversible unfolding profiles with GdmCl were also very similar in the absence and presence of 50 μM GTP plus 1 mM $MgCl_2$, with a $[GdmCl]_{1/2}$ value of 3.1 M (supplementary Figure 1); this is compatible with the release of the nucleotide at lower GdmCl concentration (48).

Nucleotide binding would be expected to stabilize the protein against denaturation. This was examined by differential scanning calorimetry which was done with GDP, in order to avoid FtsZ polymerization and GTP hydrolysis at high temperatures. Irreversible thermograms (Figure 1A) showed that this thermophilic apo-FtsZ (T_m 90.16 ± 0.03 ºC, ΔH_D 190 ± 20 kcal/mol) is further stabilized by GDP (100 μM) which increased the temperature of the transition by 10 ºC (T_m 100.72 ± 0.09 ºC, ΔH_D 220 ± 10 kcal/mol). Magnesium (10 mM $MgCl_2$) does not significantly stabilize apo-FtsZ (T_m 90.25 ± 0.02 ºC, ΔH_D 230 ± 10 kcal/mol) but apparently induces a de-stabilization of FtsZ-GDP (FtsZ-GDP-Mg^{2+} T_m 96.2 ± 0.7 ºC, ΔH_D 190 ± 10 kcal/mol). The contribution of GDP dissociation to the denaturation enthalpy, ΔH_D, could not be estimated from these experiments, due to errors of the large denaturation enthalpy values.

Binding equilibrium of guanine nucleotides to FtsZ- The stoichiometry of nucleotide binding to apo-FtsZ was checked first. Different known concentrations of GTP, GDP, mantGTP or mantGDP were added to FtsZ and the solutions high-speed centrifuged. The free nucleotide in the protein-depleted top half of tubes was measured and the bound nucleotide calculated by difference to the total. The stoichiometry values were: 0.94 ± 0.03 GDP or GTP, 0.94 ± 0.06 mant-GDP, 0.83 ± 0.08 mant-GTP, that is, essentially one nucleotide per FtsZ.

The energetics of the interaction of apo-FtsZ (10 – 25 μM) with GDP and GTP were systematically examined by ITC. Nucleotide binding is moderately exothermic (Figure 1B, C and Table 1) and the average stoichiometry of GXP binding from ITC experiments was 0.81 ± 0.06. Binding affinity increased in the presence of the nucleotide γ-phosphate (6-fold without Mg^{2+}, 1.5-fold with Mg^{2+}), but decreased (2.5 - 10 fold) when an excess of Mg^{2+} is added to provide nucleotide·Mg^{2+} complexes. Mg^{2+} alone binds with very low affinity (Table 1).

The ITC binding measurements were made under conditions in which FtsZ does not polymerize but self-associates into dimers and trimers, in a magnesium and nucleotide insensitive manner; however, FtsZ is predictably monomeric at sub-micromolar concentrations (18). Therefore the binding affinity of [8-^{3}H]-GTP to 500 nM apo-FtsZ was also measured by protein depletion, counting the top and bottom half of each solution. The best-fitting equilibrium association constant was K_b = 700 ± 100 μM^{-1}, which decreased in excess Mg^{2+} to K_b = 90 ± 20 μM^{-1} (Figure 2A). These values are 2- to 3-fold larger than association constants estimated by ITC (Table 1). This may be due to a slightly weaker binding of the nucleotide to FtsZ oligomers and the disparity of the methods.

The average of the best-fitting stoichiometries was 0.9 ± 0.1 [8-^{3}H]-GTP per FtsZ.

In order to conveniently measure the binding of nucleotides to FtsZ monomers with fluorescent methods, we employed the analogs mant-GTP and mant-GDP that contain a methyl-anthraniloyl group attached to the ribose moiety and have been widely employed to study nucleotide binding by proteins (49-51) and were found to bind specifically to FtsZ. Addition of apo-FtsZ produced both a 3.5-fold increase of the mant-nucleotide fluorescence intensity and a shift of the emission maximum from 449 nm to 440 nm. Magnesium in the millimolar concentration range quenched the fluorescence of FtsZ-bound mant-GXP, but not that of free mant-GXP. This impeded intensity measurement of the equilibrium binding of the fluorescent nucleotides to FtsZ in Mg^{2+} containing buffers. However, a protein concentration-dependent increment of anisotropy, Δr, over that of the free fluorophore (0.04) was also observed, with a maximum value, Δr_{max}, practically insensitive to Mg^{2+}. Titration of mant-GTP with apo-FtsZ in 10 mM $MgCl_2$ allowed determination of best-fitted values of Δr_{max} = 0.24 ± 0.01 and K_b = 4.2 ± 0.4 μM^{-1} (Figure 2B); titration of apo-FtsZ with mant-GTP, employing the Δr_{max} value, gave a coincident K_b value (4 ± 1 μM^{-1}) and a stoichiometry of 1.12 ± 0.06 mant-GTP bound per FtsZ (Figure 2C). Affinities of binding of mant-GDP and mant-GTP to FtsZ were systematically measured under several conditions (Table 2, supplementary Figure 2). Apparent affinities of mant derivatives are 3- to 16-fold lower than those of natural nucleotides. Triphosphate/diphosphate affinity ratios are small, and a similar weakening effect of Mg^{2+} is observed. Smaller Mg^{2+} concentrations (50 nM – 100 μM in buffer without EDTA) did not increase the apparent affinity of mant-GTP. On the other hand, the minor differences found between values measured at 25 or 55 ºC can be explained by the small binding enthalpies of GTP and GDP measured by ITC.

Finally, affinities of binding of natural guanine nucleotides to FtsZ were measured by competition with mant-GTP in the presence of Mg^{2+} (Figure 3A). K_b values for GTP, GDP and GMP were 330 ± 80, 110 ± 40 and 0.022 ± 0.007 μM^{-1} respectively. The K_b value of GTP determined by competition is 3.6-fold larger than the one determined directly by [8-^{3}H]-GTP co-sedimentation with FtsZ. The relative affinity of FtsZ for GTP and GDP was measured directly by incubating apo-FtsZ with nucleotide mixtures of varying GDP/GTP ratios, separating and quantifying the protein-bound nucleotides. The affinity of GTP binding is slightly larger than GDP binding, 11 ± 1 and 3.2 ± 0.3 fold with 0 mM and 10 mM Mg^{2+}, respectively (Figure 3B).

Kinetics of nucleotide interactions with unassembled FtsZ– The kinetics of mant-GXP binding and dissociation from FtsZ were studied by employing stopped-flow methods at 25 °C (in the presence and absence of magnesium) and at 55 °C (without magnesium to avoid polymer formation). To measure the association under pseudo-first-order conditions, mant-nucleotide was mixed with a large excess of apo-FtsZ and the increments in fluorescence intensity (Figure 4A) and anisotropy (Figure 4B) of mant were recorded. The reaction time courses were fitted by single exponentials. The rate constant values determined by intensity and anisotropy were identical within experimental error, although the noise was smaller for the intensity measurements (and it could be further reduced by removing the polarizers). The small increase in fluorescence intensity with 10 mM $MgCl_2$ could also be monitored with the stopped-flow instrument. The observed rate constant values, k_{app}, depend linearly on the concentration of binding sites (apo-FtsZ) (Figure 4C), which is compatible with a one-step binding mechanism, for which the relationship holds:

$$k_{app} = k_+[protein] + k_- \quad [1]$$

We could determine the association rate constant, k_+, from the slope of the regression line, but not, with sufficient precision, the dissociation rate constant k_-. The association rate constant is reduced by Mg^{2+} and increases weakly with temperature (Table 3).

The dissociation rate was determined in displacement experiments in which an excess of unlabeled GTP was used to displace mant-GXP from its complex with FtsZ. Time courses of mant-GXP dissociation monitored by the decrease in fluorescence intensity could be fitted to single exponentials (Figure 5) giving the first-order dissociation-rate constant values (Table 3). The dissociation rate was increased by Mg^{2+} and temperature. Calculation of equilibrium binding constants from the association and dissociation-rate constants ($K_b = k_+ / k_-$) gives values within a factor of two from the measured equilibrium values (Table 2). This supports the simple

kinetic mechanism here proposed for binding of nucleotide to unassembled FtsZ. Under conditions for FtsZ polymerization (Mg^{2+}, 55 °C), and depending on the protein concentration, both association and dissociation became multiphasic; their kinetics are analyzed next.

Kinetics of nucleotide binding and dissociation from FtsZ polymers– The interaction kinetics of mant-nucleotides with FtsZ polymers were compared with the interaction kinetics of unassembled protein. The experiments were facilitated by polymerization of nucleotide-free FtsZ (20), although a complete kinetic analysis is hampered by the system heterogeneity, consisting of unassembled FtsZ (monomers and oligomers) and FtsZ polymers.

FtsZ polymer stability was examined first. Polymerization measurements with 10 mM $MgCl_2$ at 55 °C showed that apo-FtsZ formed pelletable polymers above a critical protein concentration Cr = 7.0 ± 0.5 μM, FtsZ-mant-GTP with Cr = 2.2 ± 0.2 μM, very similar to FtsZ-GTP with Cr = 2.2 ± 0.1 μM (Figure 6A). The rate constant of GDP-induced depolymerization of apo-FtsZ, mant-GTP-FtsZ and GTP-FtsZ polymers were respectively 2.6 ± 0.1 s^{-1}, ~0.055 s^{-1} and 0.42 ± 0.05 s^{-1}. Measurements of depolymerization rates by dilution in buffer without GDP were carried out in parallel (Figure 6B) and gave the observed values of 0.16 ± 0.02 s^{-1} (apo-FtsZ), 0.03 ± 0.01 s^{-1} (mant-GTP-FtsZ) and 1.2 ± 0.1 s^{-1} (GTP-FtsZ). FtsZ-mant-GTP polymers were observed under the electron microscope and their morphology was found to be similar to that of GTP polymers. However, no polymers were detected with mant-GDP and up to 20 μM FtsZ by pelleting or electron microscopy. These observations resemble previous ones with GTP and GDP (18,20). Apo-FtsZ polymers bind mant-GTP in a molar ratio 1.0 ± 0.1, determined by sedimentation of polymers at different times after adding mant-GTP and measuring protein and mant-GTP concentrations in the pellet and in the supernatant. These polymers were stable for at least 30 minutes after adding equimolar mant-GTP, suggesting that FtsZ very slowly hydrolyzes mant-GTP, in contrast with GTP which is required in a larger excess to maintain the polymers. The hydrolysis rate of mant-GTP (20 μM) to mant-GDP by polymers of FtsZ (12 μM) was 4 x 10^{-5} s^{-1}, 10 mM $MgCl_2$ at 55 °C, (determined by HPLC), whereas the hydrolysis rate of GTP is 0.1 s^{-1} under related conditions (19).

Once the FtsZ polymer stability was determined, we proceeded to measure the mant-nucleotide association. Binding of mant-GTP to unassembled and polymerized apo-FtsZ were first compared during the same experiment (with 10 mM $MgCl_2$ at 55 °C) by loading, in the thermostated syringe of the stopped-flow instrument, either unassembled apo-FtsZ (3 μM, under the 7.0 μM Cr of polymer formation) or partially polymerized apo-FtsZ (15 μM) and then mixing it with the ligand to the same final concentration (1.5 μM). Nucleotide binding to the FtsZ polymer-containing solution was markedly slower than to unassembled FtsZ (note that the fast initial rise was smaller). Interestingly, both were complete within a few seconds and were clearly faster than the dilution-induced depolymerization measured in the same experiment (Figure 7A); this is a model-free observation. The time courses in these experiments were best fitted by a sum of three exponentials. The slowest of them was independent of protein concentration and had a constant rate value of 0.42 ± 0.05 s^{-1}. This phase was attributed to an uncharacterized rearrangement of the system and its value was constrained in further analysis. The apparent rate constants of the fastest and second-fastest phases in this experiment (Figure 7A) were: unassembled, ~70 s^{-1} and 4.6 s^{-1}; polymerized, ~40 s^{-1} and 4.3 s^{-1}. Their relative amplitudes were 10:1 in the unassembled sample and 0.4:1 in the polymerized sample. This suggests parallel reactions with two types of binding sites, fast (unassembled) and slow (polymerized FtsZ), present in different proportions in each sample. To estimate the bimolecular rate constants of binding of mant-nucleotides to unassembled and polymerized FtsZ, apo-FtsZ solutions were mixed at different final concentrations in excess over the nucleotide, time courses fitted as above and observed rates plotted against total protein concentration (Figure 7B, C). The results (Table 4) indicate that unassembled apo-FtsZ binds mant-GTP with a rate constant $k_1 \approx 30\ \mu M^{-1}s^{-1}$. This fast rate is twice the rough value predicted from measurements under related conditions (Table 3). The equivalent fast component which is observed with decreased amplitude in polymerized apo-FtsZ solutions (Table 4) can be attributed to the fraction of unassembled protein. It may then be proposed that the second rate constant, $k_2 \approx 1\ \mu M^{-1}s^{-1}$, whose amplitude

increases upon FtsZ polymerization (Table 4), reflects the binding of mant-GTP to apo-FtsZ polymers. This process is more than one order of magnitude slower than the binding to unassembled apo-FtsZ (the fact that this slow component can also be detected in a small proportion at FtsZ concentrations below the Cr measured by sedimentation might be explained by formation of polymer nucleation species which fail to pellet). Apparent rates of binding of mant-GDP and mant-GTP to polymerized apo-FtsZ were similar (Figure 7C). The inherent limitations of this phase analysis should be kept in mind, including the possibility that we are approximating a continuum of reaction rates from diverse unassembled and polymeric FtsZ species with a simple sum of a few exponentials. The dissociation rate of mant-GTP from unassembled FtsZ under polymerization conditions, ~40 s^{-1}, estimated from the y-axis intercepts in Figure 7B, C, is compatible with rough predicted values (Table 3); the dissociation rate from polymers could not be determined by this method.

Following the analysis of binding kinetics, the dissociation of mant-nucleotide from unassembled FtsZ, oligomers and FtsZ polymers were compared. To do this, mant-GXP-FtsZ was mixed with a large excess of GDP or GTP in the stopped-flow, with a minimal (10%) dilution of protein to avoid depolymerization. Dissociation of mant-GTP and mant-GDP from unassembled FtsZ (0.55 μM initial concentration, well below the 2.2 μM Cr for polymerization) took place with rate constants ~20 and ~50 s^{-1} respectively (Table 5, supplementary Figure 3), which are compatible with predicted values (Table 3). Dissociation of mant-GDP from oligomeric FtsZ (10 μM FtsZ-mant-GDP initial concentration) included a principal component with a rate constant of 0.20 s^{-1} (Table 5, suppl. Figure 3) possibly due to the FtsZ oligomers. Dissociation of mant-GTP was found to be markedly slower in polymerized FtsZ solutions (10 μM FtsZ-mant-GTP initial concentration, well above the 2.2 μM polymerization Cr). In an excess of GTP, dissociation consisted of two phases (0.018 ± 0.001 s^{-1}, 85% amplitude; 0.20 ± 0.01 s^{-1}, 15% amplitude). It was followed by partial depolymerization at a rate of 0.012 ± 0.001 s^{-1} (Figure 8, trace 1 and Table 5) and by new GTP-induced polymerization at longer times (not shown). These results indicate that mant-GTP-FtsZ polymers depolymerize upon substitution of the fluorescent derivative by GTP, suggesting that GTP-FtsZ and mant-GTP-FtsZ do not freely co-polymerize into exactly the same polymer, possibly due to some structural perturbation induced by the fluorescent group, which also inhibits the nucleotide hydrolysis. With an excess of GDP, mant-GTP dissociation proceeded at a rate of ~0.057 s^{-1} (which could not be fitted by a sum of exponentials) and was closely followed by depolymerization at ~0.055 s^{-1} monitored by light scattering (Figure 8, trace 2 and Table 5). Since dilution-induced depolymerization takes place in a similar time-scale (see above), an experimental comparison of dissociation from unassembled and polymerized FtsZ at the same final low protein concentration (as in the case of the association) could not be made.

The 0.02-0.06 s^{-1} mant-GTP dissociation rate, which may be attributed to FtsZ polymers, is several hundred-fold slower than dissociation from unassembled FtsZ under the same solution conditions. These results could be interpreted as either a lower intrinsic dissociation rate of mant-GTP from FtsZ polymers or as the result of a rate-limiting exchange of FtsZ monomers in these polymers, followed by fast nucleotide dissociation from the unassembled subunits. It should be kept in mind that this, necessarily simplified, analysis only partially resolves the dissociation rates of the nucleotide from the multiple FtsZ species present.

Accessibility of the nucleotide binding site in stable sheet of FtsZ-W319Y-His$_6$- In order to probe the accessibility of the nucleotide binding site in FtsZ polymers without the complications due to subunit exchange, it was desirable to use stabilized FtsZ polymers. Under standard conditions, histidine tagged FtsZ-His$_6$ polymerizes, hydrolyzes GTP and depolymerizes similarly to FtsZ, but large stable sheets are formed by the non-hydrolyzing point mutant FtsZ-W319Y-His$_6$ (19), which were employed as stable model FtsZ polymers. X-ray structures of FtsZ-W319Y and FtsZ-His$_6$ are superimposable (22). The FtsZ-W319Y-His$_6$ sheets are made up of double protofilaments with the same 4 nm tubulin-like subunit spacing as in wild-type FtsZ filaments. They hardly disassemble with an excess GDP or in the cold (19). Polymerized apo-FtsZ-W319Y-His$_6$ readily binds mant-GTP, with a marked increase in fluorescence intensity of the ligand; addition of an excess GTP reduced fluorescence to the level of free mant-GTP (Figure 9A). Both mant-GTP association and dissociation were essentially

complete (> 90%) within the dead time of measurement (~20 seconds, therefore proceeding at an apparent rate > 0.1 s^{-1}). This implies, for the reactant concentrations employed (12.5 μM mant-GTP and ~6 μM polymerized FtsZ-W319Y-His_6, determined by sedimentation) a bimolecular association constant > 0.05 $\mu M^{-1}s^{-1}$ for the slowest FtsZ species (52), and a dissociation constant > 0.1 s^{-1}. These rate constant are compatible with the corresponding values for wild-type FtsZ polymers (Table 5). The association time-course of 0.4 μM mant-GTP to 9 μM apo-FtsZ-W319Y-His_6 (~4 μM polymers) (Figure 9B) was biphasic, with apparent rate constants of 8.7 ± 0.2 s^{-1} (48%) and 0.290 ± 0.003 s^{-1} (52%) which may be assigned to FtsZ-W319Y-His_6 monomer and polymer respectively. The dissociation time course could not be measured due to destruction of the FtsZ-W319Y-His_6–mant-GTP polymers in the stopped-flow.

In order to estimate the rate of subunit exchange in the polymers of FtsZ-W319Y-His_6, a small proportion (5%) of tracer FtsZ-His_6 was added to the solution of preformed polymers. FtsZ-His_6 (in a 1-10% proportion) had been observed to freely copolymerize with FtsZ-W319Y-His_6 (from which it can be distinguished by fluorescence of the single tryptophan W319) without significantly perturbing polymer formation. The exchange process was very slow (Figure 9C), with an observed rate constant 0.0004 s^{-1} which clearly cannot account for the much faster observed binding of the mant-nucleotide (apparent rate > 0.1 $s\text{-}^{1}$). Finally, mant-GTP binding results were complemented by independent measurements of the exchange of α-^{32}P-GTP into unassembled and polymerized FtsZ-W319Y-His_6 and FtsZ-His_6, which exchanged one GTP in less than 20 s in all cases (Figure 9D). It can therefore be concluded that the nucleotide binding site is accessible in FtsZ-W319Y-His_6 stable model polymers.

DISCUSSION

Energetics of nucleotide binding to FtsZ and functional consequences- Guanine nucleotide binding and dissociation are central to the dynamics of FtsZ and tubulin polymers, which are in turn essential for their respective cellular functions. Thermophilic apo-FtsZ from *M. jannaschii* was employed in this work as a conveniently stable model protein for the study of the interactions of FtsZ with nucleotides. Similar experiments with nucleotide-free mesophilic FtsZ from *E. coli* were precluded by its instability. GDP stabilizes FtsZ against thermal denaturation. The destabilizing effect of Mg^{2+} on FtsZ-GDP may be explained by a reduction in the binding affinity of GDP (see below); alternately, the cation may be increasing the rate of irreversible thermal denaturation of the protein and therefore decreasing the apparent Tm. GTP binding imperceptibly modifies the average secondary structure of the protein, in agreement with the similar polymerization properties (20) and crystal structures of the nucleotide-free and GTP-liganded forms of this FtsZ (22). These results support the notion that the bound nucleotide has little structural role in *M. jannaschii* FtsZ monomers and polymers, but it is employed to trigger disassembly upon hydrolysis (20).

Apo-FtsZ binds guanine nucleotides with relatively high affinity. K_b values ranging from 20 to 300 μM^{-1}, weakly increased with the presence of the nucleotide γ-phosphate and decreased with a chelating Mg^{2+} ion (Table 1). An equivalent effect is observed with mant-GDP and mant-GTP (Table 2). $MgCl_2$ moderately reduces the association rates and enhances the dissociation rates of mant-GDP and mant-GTP (Table 3). These results indicate that the Mg^{2+} ion bound to the nucleotide β– and γ–phosphates and Gln75 observed in the crystal structure of FtsZ (22), suggested to assist the hydrolysis of the γ phosphate by FtsZ polymers, provides little additional stability to the FtsZ monomer-nucleotide complex. This may be explained by i) Mg^{2+} binding to other low affinity site that has to be displaced by the nucleotide binding or that allosterically weakens the observed nucleotide binding affinity, or ii) the existence of a slightly unfavorable process that makes the binding of the nucleotide·Mg^{2+} complex less favorable than the binding of the nucleotide alone. The first explanation is consistent with the quenching of the fluorescence of FtsZ-bound mant-GXP (Results) induced by Mg^{2+}, and with the low affinity binding of Mg^{2+} to tubulin (53). The second explanation would be compatible with a change in protonation upon Mg^{2+} binding, or with the introduction of some strain by the binding of Mg^{2+} to the FtsZ-GTP complex.

FtsZ and tubulin form a distinct family of GTPases (1), but there are structural (22) and important functional differences between the FtsZ and tubulin nucleotide binding sites. Unlike

FtsZ, nucleotide γ-phosphate and Mg^{2+} binding are linked in αβ–tubulin (54). The nucleotide γ-phosphate and the coordinated Mg^{2+} ion bound at the functional GTP/GDP binding site of β-tubulin control microtubule stability, whereas the Mg^{2+} bound to the non-functional GTP site of α-tubulin controls the stability of the αβ-dimer (55). In classical GTPases, GTP is bound in complex with Mg^{2+}, which is coordinated to oxygens from the β- and the γ-phosphates. However, the functional roles of the γ-phosphate and Mg^{2+} vary among different G-proteins. Thus, Ras and EF-Tu form tight GDP·Mg complexes; Mg^{2+} binding reduces the GDP off rate by four orders of magnitude and GDP binds more tightly than GTP (56). For another example, Mg^{2+} is not required for GDP binding to eRF3 but strengthens GTP binding; no structural changes were observed for GTP·Mg^{2+} and GDP·Mg^{2+} binding to eRF3 (57). In Rho proteins, the Mg^{2+} cofactor does not affect the nucleotide binding affinity *per se*, but rather, acts as a kinetic stabilizer for bound nucleotides by slowing down both the off and on rates (58). The different properties of the FtsZ nucleotide binding site in comparison with tubulin and other GTPases suggest the possibility of fine-tuning specific inhibitors for the FtsZ-GTP interaction.

Interactions of FtsZ monomers with fluorescent mant-nucleotides, kinetics of binding and competitive assay for ligands of the FtsZ nucleotide site- Interactions of FtsZ monomers with GTP and GDP were probed by employing the fluorescence anisotropy change of their mant derivatives in dilute solutions. The kinetics of association of mant-nucleotides to unassembled FtsZ is compatible with a one-step reaction, with fast association rate constant values ($10 < k_+ < 40\ \mu M^{-1}\ s^{-1}$) and dissociation rates ($1 < k_+ < 10\ s^{-1}$), depending on solution conditions (Table 3). Rate constant values are weakly dependent on temperature, suggesting small activation energies for nucleotide association and dissociation from an easily accessible site.

The bound mant-GTP is specifically displaced by non-fluorescent nucleotides. Except for the possible offset in absolute K_b values determined by competition and ITC methods, the ratio K_b (GTP-Mg^{2+}) / K_b (GDP-Mg^{2+}) determined with the competition method is 3 ± 2, which is comparable to the 3.2 ± 0.3 ratio directly determined with GTP and GDP (Figure 3B), to the ~1.5 ratio from ITC (Table 1), and to the 2.6 ± 0.6 ratio of the respective mant-derivatives (Table 2).

The mant-nucleotide displacement method outlined here is a homogeneous fluorescence assay which may, in principle, be conveniently employed to characterize the binding of any nucleotides or other substances, such as small molecule modulators of FtsZ assembly (Introduction), to its nucleotide site, as well as to measure the effects of ligand modifications on binding affinity. This method may be eventually scaled up to screen for inhibitors binding to the FtsZ nucleotide site.

Exchangeable nucleotide is kinetically stabilized in FtsZ polymers- How FtsZ polymers exchange the hydrolyzed nucleotide is a major unresolved issue, which impacts on the mechanism of their dynamics being possibly different or similar to microtubules (Introduction). The results of this study indicate that the nucleotide remains exchangeable in polymers of FtsZ from *M. jannaschii*. The accessibility of the nucleotide binding site in FtsZ polymers was probed by measuring the kinetics of interactions of FtsZ with mant-GTP under polymerization conditions. The scheme in Figure 10A summarizes relevant rate constants determined with unassembled FtsZ (at protein concentrations below Cr) and estimated for FtsZ polymers (above Cr). The apo-FtsZ polymers are obviously devoid of any dynamics related to nucleotide hydrolysis and FtsZ-mant-GTP polymers do not hydrolyze the nucleotide on the time scale of these experiments. Under polymerization conditions, binding kinetics becomes multiphasic due to the different FtsZ aggregation species found in solution. A nucleotide association phase with a rate constant 1 $\mu M^{-1}s^{-1}$, whose amplitude increases upon polymerization (Results), was ascribed to the binding of mant-GTP to FtsZ polymers, 30-fold slower than to unassembled FtsZ. This binding rate constant cannot come from the dissociation of apo-FtsZ subunits nor from nucleotide binding to the unassembled protein, since the apo-FtsZ polymer dissociation rate is much lower than the observed mant-GTP binding rates (Figure 7).

Dissociation of mant-GTP from FtsZ polymers proceeds at an observed rate of 0.06 s^{-1} in GDP excess (0.02 s^{-1} in GTP excess), which is three orders of magnitude slower than dissociation from unassembled FtsZ. The value of 0.21 s^{-1} estimated for mant-GTP dissociation from FtsZ polyers using the rate and equilibrium

constants depicted in the reaction box of Figure 10A is only 3.5-fold higher (not too bad considering the difficulty of several of the kinetic measurements). The fact that the mant-GTP dissociation time course shortly precedes polymer disassembly (Figure 8) would be compatible with direct dissociation of mant-GTP from the polymer, closely followed by disassembly of the GDP-bound polymer at the rates indicated (Figure 10A), However, we do not think that monitoring the polymer concentration by scattering is accurate enough to warrant this interpretation. Given the similarity of the apparent ligand dissociation rate and the polymer disassembly rate, this result may also be interpreted as due to FtsZ depolymerization followed by fast mant-GTP dissociation from FtsZ monomers. According to this interpretation the 0.06 s^{-1} value would be only an upper limit to the true rate constant of mant-GTP dissociation from the polymers. The slower dissociation rate in excess of GTP indicates the participation of polymer disassembly in this process. In either case, our results indicate that the nucleotide is kinetically stabilized in FtsZ polymers with respect to monomers. This agrees with an accessible nucleotide binding site located between two consecutive monomers along the FtsZ protofilament (22). Mant-GTP binding and FtsZ polymer elongation moderately favor each other, with a linkage free energy of only -1.1 ± 0.4 kcal mol^{-1}, calculated from data in Figure 10A.

In order to unequivocally prove whether FtsZ polymers can bind and dissociate nucleotide without subunit exchange, stabilized FtsZ polymers were needed. These have been provided by the mutant FtsZ-W319Y-His_6, which forms inactive GTPase sheet (further stabilized by the His tag, (19)) and co-polymerizes with wild-type FtsZ-His_6. Wild-type subunits slowly exchange into mutant polymers at a rate of 0.0004 s^{-1}, whereas polymers bind and dissociate mant-GTP nucleotide at a much faster rate, > 0.1 s^{-1}, under the same conditions. This shows that exchange of the bound nucleotide without subunit exchange is possible in these model FtsZ polymers.

Implications for FtsZ polymer dynamics- The observation that mant-nucleotide exchange can take place without hydrolysis in polymers of *M. jannaschii* FtsZ gives insight into FtsZ polymer dynamics. These results might superficially seem to favor models in which FtsZ is devoid of any microtubule-like dynamics. However, the problem is quantitative: the kinetic pathway actually operative will depend on the effective reaction rates under given conditions. Once FtsZ polymers eventually hydrolyze mant-GTP and release Pi, mant-GDP would be expected to induce disassembly, but, since mant-GTP hydrolysis is much slower that the mant-nucleotide exchange, it does not influence polymer dynamics. This is not the case with the natural nucleotide GTP. Models for FtsZ assembly with GTP are schematized in Figure 10B. *M. jannaschii* FtsZ polymers hydrolyze GTP with a turnover of 0.10 s^{-1} (19), which is similar to the value of 0.07 s^{-1} reported for *E. coli* FtsZ, at lower temperature (21). *M. jannaschii* FtsZ polymers disassemble rapidly, with half-times of 0.6 s (FtsZ-GTP polymers) to 25 s (mant-GTP-FtsZ polymers); these values comprise the 5 s half-time for *E. coli* FtsZ polymer disassembly (in GDP excess) and the 7 s half-time of subunit exchange, reported under quite different conditions (25). GDP dissociation from FtsZ polymers, which is difficult to measure, is rate limiting to the exchange of GTP into polymers. If it is faster than the rate of hydrolysis, the steady-state polymer may contain mainly GTP and a minor fraction of GDP-bound subunits; which will have a given probability of fragmenting the polymer. As long as the nucleotide exchange in the polymer is significantly faster than hydrolysis and disassembly, subunit turnover is expected to be independent of the GTPase rate. On the contrary, if GDP dissociation is slower than GTP hydrolysis, GDP-bound subunits will accumulate and the polymer will disassemble. Subunits will then rapidly exchange nucleotide with the solution and recycle into new polymers (indicated by the circular arrow in Figure 10B). In this case subunit turnover is expected to depend on the GTPase rate. A steady-state population of recycling FtsZ polymers will contain mainly GTP polymers and a small fraction of GDP-containing FtsZ polymers. An estimate for the dissociation rate of GDP-FtsZ polymers is provided by the observed GDP-induced dissociation rate constant (2.6 s^{-1}) of apo-FtsZ polymers assuming that the binding of GDP is not rate-limiting.

The observation that subunit exchange is very slow in polymers of the GTPase deficient mutant FtsZ-W319Y-His_6 (Figure 9) compared to the fast disassembly of FtsZ-His_6 active GTPase (19) and the important findings that i) the turnover of FtsZ-GFP subunits in the Z-rings

of *E. coli* cells is reduced in mutant *ftsZ84*, which has a slow GTPase *in vitro* (23,24), ii) FtsZ subunit exchange in FRET assay is strongly reduced by the slowly hydrolysable nucleotide GMPCMP (25) and iii) the correlation very recently found, between the slower subunit turnover, GTPase and GDP-induced disassembly in *Mycobacterium tuberculosis* FtsZ (26) do favor a polymer recycling model of FtsZ assembly (Figure 10B). In conclusion, FtsZ polymers can be observed to exchange nucleotide, unlike microtubules, but GDP dissociation may be slow enough for FtsZ polymer disassembly to take place first, as in microtubules, resulting in FtsZ polymers cycling with GTP hydrolysis. Since FtsZ polymers are typically single flexible protofilaments a few hundred nanometer long (Huecas, unpublished), it is possible that their relatively rapid assembly and disassembly does not produce work, but proceeds between membrane attachment points and provides continuously updated positional information for the assembly and operation of the septosome.

Acknowledgments. We thank Martín Alba for FtsZ purification and Dr. Jesús Mingorance for help with the α-^{32}P-GTP filtration assay. This work was supported in part by grants MEC BFU 2005-00505/BMC (JMA), MEC BFU-2006-10288 (MM), grant CAM S-BIO-0214-2006 (JMA, JFD), a CSIC-I3P postdoctoral contract (SH), a MEC-FPI predoctoral fellowship (CS) and a travel grant FAPESP CBME - 98/14138-2 (WG).

REFERENCES

1. Nogales, E., Downing, K. H., Amos, L. A., and Lowe, J. (1998) *Nat Struct Biol* **5**, 451-458
2. Aldaz, H., Rice, L. M., Stearns, T., and Agard, D. A. (2005) *Nature* **435**, 523-527
3. Schlieper, D., Oliva, M. A., Andreu, J. M., and Lowe, J. (2005) *Proc Natl Acad Sci U S A* **102**, 9170-9175
4. Sontag, C. A., Staley, J. T., and Erickson, H. P. (2005) *J Cell Biol* **169**, 233-238
5. Larsen, R. A., Cusumano, C., Fujioka, A., Lim-Fong, G., Patterson, P., and Pogliano, J. (2007) *Genes Dev* **21**, 1340-1352
6. Bi, E. F., and Lutkenhaus, J. (1991) *Nature* **354**, 161-164
7. Rothfield, L., Taghbalout, A., and Shih, Y. L. (2005) *Nat Rev Microbiol* **3**, 959-968
8. Michie, K. A., and Lowe, J. (2006) *Annu Rev Biochem* **75**, 467-492
9. Vicente, M., and Rico, A. I. (2006) *Mol Microbiol* **61**, 5-8
10. Lutkenhaus, J. (2007) *Annu Rev Biochem* **76**, 539-562
11. Weart, R. B., Lee, A. H., Chien, A. C., Haeusser, D. P., Hill, N. S., and Levin, P. A. (2007) *Cell* **130**, 335-347
12. Buey, R. M., Diaz, J. F., and Andreu, J. M. (2006) *Biochemistry* **45**, 5933-5938
13. Thanbichler, M., and Shapiro, L. (2006) *Cell* **126**, 147-162
14. Chung, K. M., Hsu, H. H., Yeh, H. Y., and Chang, B. Y. (2007) *J Biol Chem* **282**, 14891-14897
15. Nogales, E. (1999) *Cell Mol Life Sci* **56**, 133-142
16. Burbank, K. S., and Mitchison, T. J. (2006) *Curr Biol* **16**, R516-517
17. Mingorance, J., Rueda, S., Gomez-Puertas, P., Valencia, A., and Vicente, M. (2001) *Mol Microbiol* **41**, 83-91
18. Huecas, S., and Andreu, J. M. (2003) *J Biol Chem* **278**, 46146-46154
19. Oliva, M. A., Huecas, S., Palacios, J. M., Martin-Benito, J., Valpuesta, J. M., and Andreu, J. M. (2003) *J Biol Chem* **278**, 33562-33570
20. Huecas, S., and Andreu, J. M. (2004) *FEBS Lett* **569**, 43-48
21. Romberg, L., and Mitchison, T. J. (2004) *Biochemistry* **43**, 282-288
22. Oliva, M. A., Cordell, S. C., and Lowe, J. (2004) *Nat Struct Mol Biol* **11**, 1243-1250
23. Stricker, J., Maddox, P., Salmon, E. D., and Erickson, H. P. (2002) *Proc Natl Acad Sci U S A* **99**, 3171-3175

24. Anderson, D. E., Gueiros-Filho, F. J., and Erickson, H. P. (2004) *J Bacteriol* **186**, 5775-5781
25. Chen, Y., and Erickson, H. P. (2005) *J Biol Chem* **280**, 22549-22554
26. Chen, Y., Anderson, D. E., Rajagopalan, M., and Erickson, H. P. (2007) *J Biol Chem* **282**, 27736-27743
27. Vollmer, W. (2006) *Appl Microbiol Biotechnol* **73**, 37-47
28. Lappchen, T., Hartog, A. F., Pinas, V. A., Koomen, G. J., and den Blaauwen, T. (2005) *Biochemistry* **44**, 7879-7884
29. Paradis-Bleau, C., Beaumont, M., Sanschagrin, F., Voyer, N., and Levesque, R. C. (2007) *Bioorg Med Chem* **15**, 1330-1340
30. Ohashi, Y., Chijiiwa, Y., Suzuki, K., Takahashi, K., Nanamiya, H., Sato, T., Hosoya, Y., Ochi, K., and Kawamura, F. (1999) *J Bacteriol* **181**, 1348-1351
31. Wang, J., Galgoci, A., Kodali, S., Herath, K. B., Jayasuriya, H., Dorso, K., Vicente, F., Gonzalez, A., Cully, D., Bramhill, D., and Singh, S. (2003) *J Biol Chem* **278**, 44424-44428
32. Santra, M. K., Beuria, T. K., Banerjee, A., and Panda, D. (2004) *J Biol Chem* **279**, 25959-25965
33. Margalit, D. N., Romberg, L., Mets, R. B., Hebert, A. M., Mitchison, T. J., Kirschner, M. W., and RayChaudhuri, D. (2004) *Proc Natl Acad Sci U S A* **101**, 11821-11826
34. Reynolds, R. C., Srivastava, S., Ross, L. J., Suling, W. J., and White, E. L. (2004) *Bioorg Med Chem Lett* **14**, 3161-3164
35. Urgaonkar, S., La Pierre, H. S., Meir, I., Lund, H., RayChaudhuri, D., and Shaw, J. T. (2005) *Org Lett* **7**, 5609-5612
36. Stokes, N. R., Sievers, J., Barker, S., Bennett, J. M., Brown, D. R., Collins, I., Errington, V. M., Foulger, D., Hall, M., Halsey, R., Johnson, H., Rose, V., Thomaides, H. B., Haydon, D. J., Czaplewski, L. G., and Errington, J. (2005) *J Biol Chem* **280**, 39709-39715
37. Beuria, T. K., Santra, M. K., and Panda, D. (2005) *Biochemistry* **44**, 16584-16593
38. Huang, Q., Kirikae, F., Kirikae, T., Pepe, A., Amin, A., Respicio, L., Slayden, R. A., Tonge, P. J., and Ojima, I. (2006) *J Med Chem* **49**, 463-466
39. Ito, H., Ura, A., Oyamada, Y., Tanitame, A., Yoshida, H., Yamada, S., Wachi, M., and Yamagishi, J. (2006) *Microbiol Immunol* **50**, 759-764
40. Possoz, C., Newmark, J., Sorto, N., Sherratt, D. J., and Tolmasky, M. E. (2007) *Antimicrob Agents Chemother* **51**, 252-256
41. Jaiswal, R., Beuria, T. K., Mohan, R., Mahajan, S. K., and Panda, D. (2007) *Biochemistry* **46**, 4211-4220
42. Domadia, P., Swarup, S., Bhunia, A., Sivaraman, J., and Dasgupta, D. (2007) *Biochem Pharmacol*
43. Bradford, M. M. (1976) *Anal Biochem* **72**, 248-254
44. Medrano, F. J., Andreu, J. M., Gorbunoff, M. J., and Timasheff, S. N. (1991) *Biochemistry* **30**, 3770-3777
45. Andreu, J. M., and Barasoain, I. (2001) *Biochemistry* **40**, 11975-11984
46. Diaz, J. F., and Buey, R. M. (2007) *Characterizing Ligand-Microtubule Binding by competition methods*. Microtubule Protocols (Zhou, J., Ed.), Humana Press, Totowa, New Yersey
47. Bevington, P. R. (1969) *Data reduction and error analysis for the physical sciences*, McGraw-Hill Book Co., New York
48. Andreu, J. M., Oliva, M. A., and Monasterio, O. (2002) *J Biol Chem* **277**, 43262-43270
49. Simon, I., Zerial, M., and Goody, R. S. (1996) *J Biol Chem* **271**, 20470-20478

50. Jameson, D. M., and Eccleston, J. F. (1997) *Methods Enzymol* **278**, 363-390
51. Pisareva, V. P., Hellen, C. U., and Pestova, T. V. (2007) *Biochemistry* **46**, 2622-2629
52. Barshop, B. A., Wrenn, R. F., and Frieden, C. (1983) *Anal Biochem* **130**, 134-145
53. Frigon, R. P., and Timasheff, S. N. (1975) *Biochemistry* **14**, 4567-4573
54. Correia, J. J., Baty, L. T., and Williams, R. C., Jr. (1987) *J Biol Chem* **262**, 17278-17284
55. Menendez, M., Rivas, G., Diaz, J. F., and Andreu, J. M. (1998) *J Biol Chem* **273**, 167-176
56. Sprang, S. R. (1997) *Annu Rev Biochem* **66**, 639-678
57. Kong, C., Ito, K., Walsh, M. A., Wada, M., Liu, Y., Kumar, S., Barford, D., Nakamura, Y., and Song, H. (2004) *Mol Cell* **14**, 233-245
58. Zhang, B., Zhang, Y., Wang, Z., and Zheng, Y. (2000) *J Biol Chem* **275**, 25299-25307
59. Oosawa, F., and Asakura, S. (1975) *Thermodynamics of the polymerization of protein*, Academic Press, London

FIGURE LEGEND

Fig. 1. (A), DSC traces of ApoFtsZ (12.5 μM) with $MgCl_2$ (10 mM), with GDP (100 μM) and with GDP (100 μM) plus $MgCl_2$ (10 mM) in Pipes-KCl buffer. (B) and (C), calorimetric titration (ITC) of FtsZ binding to GDP and GTP·Mg^{2+}, respectively, at 25 ºC. Each peak (upper panels) represents the heat (integrated area) resulting from ligand injection into FtsZ solution (Methods). Each point in the bottom panels is the heat evolved per mole of injected ligand in the corresponding peak in the upper panel, after subtraction of ligand dilution heat. Solid lines are the best fits to experimental data (see Table 1 for binding parameters).

Fig. 2. (A), Isotherms of binding of [8-^{3}H]-GTP to apo-FtsZ. Apo-FtsZ (500 nM) in Pipes-KCl buffer, in the absence (solid triangles) or presence of 10 mM $MgCl_2$ (solid circles) at 25 ºC. Void symbols are the [8-^{3}H]-GTP bound in the presence of an excess of GTP (200 μM). (B) and (C), Isotherms of binding of apo-FtsZ and mant-GTP, measured by fluorescence anisotropy of the ligand. (B) Titration of mant-GTP (50 nM) with apo-FtsZ (fitted Δr_{max} = 0.234 ± 0.005 was in this experiment). (C) Titration of apo-FtsZ (500 nM) with mant-GTP. Void symbols are non-specific binding, measured with an added excess of GTP (250 μM). Lines in each case are the best-fitted model isotherms (see main text for binding parameters).

Fig. 3. Relative affinity of FtsZ for guanine nucleotides. (A), Displacement curves of mant-GTP (500 nM total) from FtsZ (500 nM apo-FtsZ total) by GTP (solid circles), GDP (void circles) and GMP (squares) in Pipes-KCl buffer, 10 mM $MgCl_2$ at 25 ºC. Data were determined from the change in mant-GTP anisotropy with the competing ligands (Methods). Lines (solid, dash, dash-dot) correspond to the best fitted K_b to each data set (see Methods and Results). (B) Relative affinity of FtsZ for GTP and GDP. Apo-FtsZ (32 μM) was incubated with GTP/GDP mixtures (total GXP 200 μM) in 50 mM Tris-HCl, 50 mM KCl, 1 mM EDTA, pH 7.5, (0.5 mL) at 25 °C during 60 minutes, excess nucleotide was removed, and protein-bound nucleotides analyzed. For two ligands binding to the same site, the slope of this plot is the ratio of their equilibrium binding constants. Void triangles, no $MgCl_2$; solid triangles, 10 mM $MgCl_2$.

Fig. 4. Kinetics of binding of mant-GDP and mant-GTP to ApoFtsZ. (A) and (B), a 1 μM solution of mant-GDP was mixed with 10 μM ApoFtsZ in the stopped flow instrument at 25 ºC (final concentrations of 500 nM mant-GDP and 5 μM ApoFtsZ). Binding was followed by fluorescence intensity (A) and by anisotropy (B). Void symbols in A and B are controls of mant-GDP mixed with buffer. Solid lines are the best fits of a single exponential to experimental data (k_+ (intensity) = 101 ± 2 s^{-1}, ΔF_{max} = 2.00 ± 0.03; k_+ (anisotropy) = 110 ± 10 s^{-1}, Δr_{max} = 0.07 ± 0.005) (C), Dependence on

the concentration of apo-FtsZ of the observed rate constants of binding of mant-GDP (circles) and mant-GTP (squares) with 10 mM $MgCl_2$ (solid symbols) and without $MgCl_2$ (void symbols) at 25 ºC.

Fig. 5. Kinetics of dissociation of mant-GTP and mant-GDP from unassembled FtsZ. The mant-nucleotide-FtsZ complex was formed by adding 2 μM ApoFtsZ to 1 μM mant-GXP, with or without 10 mM $MgCl_2$. At time zero, this solution was mixed 1:1 with 400 μM GTP. The reaction was followed by the change in fluorescence of the mant-GXP (gray traces). Data were fitted to single exponentials (black lines; see rate constant values in Table 4). Trace 1, mant-GTP, 25 ºC; trace 2, mant-GDP, 25 ºC; trace 3, mant-GDP with Mg^{2+}, 25 ºC; trace 4, mant-GTP with Mg^{2+}, 25 ºC; trace 5, mant-GTP, 55 ºC; trace 6, mant-GDP, 25 ºC; trace 7, mant-GTP alone. Note that each pair of mant-GTP/mant-GDP measurements is arbitrarily displaced on the y-axis to facilitate comparison.

Fig. 6. (A), Nucleated polymerization of apo-FtsZ with mant-GTP (20 μM, solid circles), GTP (1 mM, solid triangles) or without any nucleotide (void circles) in Pipes-KCl buffer, 10 mM $MgCl_2$, at 55 ºC. The polymers formed were measured by sedimentation. (B), Kinetics of depolymerization monitored by light-scattering in the stopped-flow under the same solution conditions as in panel A. Apo-FtsZ polymers (15 μM) were diluted to 12 μM in 2 mM GDP (trace 1) or to 1.5 μM in buffer (trace 2). FtsZ-Mant-GTP polymers (15 μM) were diluted to 1.5 μM in buffer (trace 3) (for dissociation in GDP excess see dashed trace 2 in Figure 8). FtsZ-GTP polymers (15 μM) were diluted to 12 μM in 2 mM GDP (trace 4) or to 1.5 μM in buffer (trace 5).

Fig. 7. (A), Kinetics of binding of mant-GTP to unassembled (trace 1) and to polymerized (trace 2) apo-FtsZ. Polymers were formed from 15 μM apo-FtsZ with 10 mM $MgCl_2$ at 55ºC (8 μM apo-FtsZ in polymers) and mixed in the stopped-flow at final concentrations of 1.5 μM FtsZ (0.8 μM polymers) and 400 nM mant-GTP (trace 2). Light scattering was recorded during the experiment with apo-FtsZ polymers to monitor their stability (trace 3). The light scattering signal changed from 2.22 to 2.18 during the ligand binding measurement and to 2.10 later when depolymerization was complete. Unassembled apoFtsZ (3 μM, under same conditions) was mixed to 1.5 μM final concentration (trace 1). Data were fitted by a sum of three exponentials k_{1app}, k_{2app}, k_{3app}: (1) 72 s^{-1} (69%), 4.6 s^{-1} (7%) and 0.42 s^{-1} (24%); (2) 43 s^{-1} (16%), 4.3 s^{-1} (32%) and 0.42 s^{-1} (52%). Residuals of the fit are shown in the small panel above. (B), Dependence of the observed rate constants k_{1app} and k_{2app} on the concentration of unassembled apo-FtsZ (solid circles, 400 nM mant-GTP; void circles, mant-GDP shown for comparison). (C), Dependence of the observed rate constants k_{1app} and k_{2app} on the final total concentration of apo-FtsZ under polymerization conditions (400 nM mant-GXP); a very slow third rate constant k_{3app} 0.42 s^{-1} was independent of protein concentration and is not plotted.

Fig. 8. Kinetics of dissociation of mant-GTP and mant-GDP from FtsZ under polymerization conditions. Dissociation of mant-GTP from 10 μM FtsZ polymers diluted to 9 μM in 1mM GTP (line 1), 1 mM GDP (line 2) or without nucleotide (line 3). Light scattering was also recorded during the experiment to follow depolymerization (corresponding dashed lines). Residuals are of a double exponential fit to fluorescence intensity, line 1, and a single exponential fit to light scattering, line 2 (see rate values in main text; a multiple exponential did not improve fit 2).

Fig. 9. Interactions of non-hydrolyzing mutant FtsZ-W319Y-His_6 with nucleotides (A), Mant-GTP binding to polymers of FtsZ-W319Y-His_6. Solid line, fluorescence emission spectrum of 12.5 μM mant-GTP in a solution of 12.5 μM polymerized apo-FtsZ-W319Y-His_6; dashed line, mant-GTP alone; dotted line, mant-GTP + polymerized FtsZ-W319Y-His_6 + 1 mM GTP; dash-dot line, polymerized FtsZ-W319Y-His_6 alone; the spectrum of mant-GTP + GTP was identical to mant-GTP alone. Excitation was at 357 nm (1 nm banwidth); emission maxima of bound mant-GTP was at 439 nm, free at 446 nm (2 nm bandwith). Inset: an electron micrograph of the FtsZ-W319Y-His_6-mant-GTP polymers; the bar indicates 100 nm. (B), Association time course of 0.4 μM mant-GTP to 9 μM apo-FtsZ-W319Y-His_6 monitored with the stopped-flow. The grey trace are data and the dark line the bi-exponential best fit. (C), Time course of incorporation of 0.63 μM FtsZ-His6 into ~6 μM preformed polymers of the FtsZ-W319Y-His_6 Trp-less mutant (12.5 μM total concentration),

measured by polymer sedimentation. The solid line is a single exponential fit to data, giving a pseudofirst order rate constant 4 ± 1 x 10^{-4} s^{-1} and an amplitude 0.06 ± 0.01 (marked *fit*); maximum incorporation was 0.053 ± 0.003 (marked *exp*), determined by copolymerizing the FtsZ-wt-His_6 together with FtsZ-W319Y-His_6. (D), Time courses of exchange of α-^{32}P-GTP into 12.5 μM FtsZ-W319Y-His_6 (solid) circles or FtsZ-His_6 (void circles) under no assembly (left, no $MgCl_2$) or polymerization conditions (right, 6 mM $MgCl_2$), measured with a filtration assay. Note that FtsZ-His_6 polymers hydrolyze GTP while FtsZ-W319Y-His_6 ones do not.

Fig. 10. Interactions of FtsZ monomers and polymers with fluorescent and natural nucleotides

(A), Scheme of mant-GTP binding kinetics to FtsZ monomers and polymers. Exchangeable mant-GTP is kinetically stabilized in polymers of FtsZ from *M. jannaschii*. The nucleotide is represented by small black circles. Mant-GTP was not hydrolyzed during the experiments, therefore all reactions represented in this scheme are chemical equilibria. Nucleotide binding and dissociation rates were determined from fluorescence measurements in this work. Polymer dissociation rates are preliminary estimates from light scattering measurements following dilution, both with a stopped-flow instrument. Polymer elongation rates (k_+) were calculated from the critical concentration (C_r) and dissociation rate (k_-) values ($Cr = k_- / k_+$) for an end-growing nucleated polymer in equilibrium with monomers (59).

(B), Do FtsZ polymers cycle with GTP hydrolysis? In this scheme GTP and GDP are represented by small filled and void circles respectively. Nucleotide exchange by FtsZ monomers in a GTP excess is expected to be relatively fast (similarly to mant- nucleotides, Table 3) and not rate-limiting for consecutive reactions. FtsZ-GTP polymers disassemble at a relatively fast rate (upon dilution or in GDP excess). Nucleotide exchange by FtsZ polymers in a GTP excess is limited by an as-yet unknown rate of GDP dissociation from FtsZ polymers. Nucleotide exchange by the polymer has an effect opposite to that of hydrolysis. Depending on the ratio of GDP dissociation and GDP-polymer disassembly rates to the hydrolysis rate, FtsZ polymers may undergo cycles of assembly, GTP hydrolysis, disassembly and nucleotide exchange as indicated by the curved arrow.

TABLES

Table 1. Energetics of the interactions of FtsZ with nucleotides determined by ITC at 25 °C.

Ligand	K_b (μM^{-1})	ΔG_b (kcal mol^{-1})	ΔH_b (kcal mol^{-1})	ΔS_b (cal K^{-1} mol^{-1})
GDP	50 ± 10	-10.5 ± 0.1	-6.80 ± 0.20	12.4 ± 0.3
GDP-Mg^{2+}	20 ± 8	-10.0 ± 0.2	-3.78 ± 0.09	20.9 ± 0.4
GTP	300±100	-11.6 ± 0.2	-5.88 ± 0.08	19.1 ± 0.4
GTP-Mg^{2+}	30 ± 10	-10.2 ± 0.2	-3.31 ± 0.03	23.1 ± 0.6
Mg^{2+}	0.0001 ± 0.00003	-2.7 ± 0.2	4.2 ± 0.7	23 ± 2

ITC experiments were made with 0 or 10 mM $MgCl_2$ in both protein and GXP solutions (the titration with $MgCl_2$ was done without EDTA). The stoichiometry of the low affinity Mg^{2+} binding cannot be measured from these experiments and, therefore, the enthalpy change is an estimate per mole of protein, not per mole of site. Titration of FtsZ-GTP (no EDTA) with equimolar Mg^{2+} gave insignificant heat.

Table 2. Equilibrium association constants of mant-nucleotides to apo-FtsZ and their dependence on $MgCl_2$ concentration and temperature.

Nucleotide	[$MgCl_2$] (mM)	K_b (μM^{-1}), 25ºC	K_b (μM^{-1}), 55ºC
mant-GDP	0.0	17 ± 2 (19 ± 2)	10 ± 1 (18 ±3)
	2.0	10 ± 3	11 ± 1
	10.0	1.6 ± 0.2	1.4 ± 0.2
mant-GTP	0.0	18 ± 5 (32 ± 4)	35 ± 5 (21 ± 2)
	2.0	5 ± 2	5.3 ± 0.9
	10.0	4.2 ± 0.4	3 ± 1

10 nM mant-GXP was titrated with apo-FtsZ in Pipes-KCl buffer with 0, 2 or 10 mM $MgCl_2$. Free Mg^{2+} concentrations are ~ 4 nM, 1 mM and 9 mM respectively (our cation-free buffers typically contain ~ 1 μM residual Mg^{2+}). Binding was measured from the increase in fluorescence anisotropy of mant-GXP. In brackets, equilibrium constants measured by fluorescence intensity.

Table 3. Kinetics of binding and dissociation of mant-nucleotides from FtsZ.

rate constant	mant-GTP		Mant-GDP	
	25 ºC	55 ºC	25 ºC	55 ºC
k_+ ($\mu M^{-1}s^{-1}$), no $MgCl_2$	28 ± 2 (26 ± 5)	37 ± 7	25 ± 1 (23 ± 5)	35 ± 4
k_+ ($\mu M^{-1}s^{-1}$), 10 mM $MgCl_2$	12 ± 1 (11 ± 2)	~16 predicted	6 ± 1 (7 ± 2)	~7 predicted
k_- (s^{-1}), no $MgCl_2$	0.82 ± 0.01	2.25 ± 0.01	2.00 ± 0.01	11.0 ± 0.1
k_- (s^{-1}), 10 mM $MgCl_2$	6.30 ± 0.02	~17 predicted	7.17 ± 0.03	~40 predicted

Association and dissociation rate constants were determined from the fluorescence intensity change of mant-GXP in Pipes-KCl buffer; constants obtained from the anisotropy increment are indicated in brackets. Predicted values of association and dissociation rate constants in magnesium at 55ºC, obtained by multiplying the values with magnesium at 25 ºC by the ratio of values at 55 and 25 ºC without magnesium, are indicated solely for the purpose of comparison with further measurements (Table 4).

Table 4. Association kinetics of mant-GTP to apo-FtsZ under polymerization solution conditions.

initial [apo-FtsZ]	K_1 ($\mu M^{-1}s^{-1}$) (unassembled)	k_{-1} (s^{-1}) (unassembled)	k_2 ($\mu M^{-1}s^{-1}$) (polymer)	k_3 (s^{-1}) (unknown)
below Cr for polymerization	30 ± 6 (49 ± 8%)	38 ± 7	1 ± 2 (7 ± 3%)	0.42 ± 0.05 (44 ± 10%)
above Cr for polymerization	35 ± 15 (24 ± 10%)	44 ± 20	1.1 ± 0.3 (20 ± 6%)	0.42 ± 0.05 (56 ± 8%)

Values in parenthesis are the average relative amplitude of each phase. Association values from apo-FtsZ above Cr have been corrected by the fractions of unassembled and polymeric FtsZ in solution. Available mant-GDP data are roughly similar to the mant-GTP data (Figure 7B, C).

Table 5. Observed dissociation rate constants (s^{-1}) of mant-GXP from FtsZ under polymerization solution conditions.

initial conditions	k_{-1} (GDP excess)	k_{-2} (GDP excess)	k_{-1} (GTP excess)	k_{-2} (GTP excess)
Unassembled mant-GDP-FtsZ (0.5 μM FtsZ)	53 ± 8	NO	52 ± 9	NO
Unassembled mant-GTP-FtsZ (0.5 μM FtsZ)	22 ± 2	NO	18 ± 3	NO
mant-GDP-FtsZ oligomers (9 μM FtsZ)	40 ± 10 (10 %)	0.20 ± 0.05 (90%)	33 ± 10 (10 %)	0.21 ± 0.05 (90 %)
mant-GTP-FtsZ polymers (9 μM FtsZ)	NO	0.057 ± 0.005	0.20 ± 0.01 (15%)	0.018 ± 0.001 (85%)

Apo-FtsZ with added mant-GTP or mant-GDP (1.1 nucleotide:1 FtsZ) was allowed to polymerize at 55 ºC with 10 mM $MgCl_2$ and mixed in the stopped-flow with an excess (1 mM) GTP or GDP as indicated. The reaction time courses were recorded during 400 s. NO, a second phase was not observed.

Figure 1

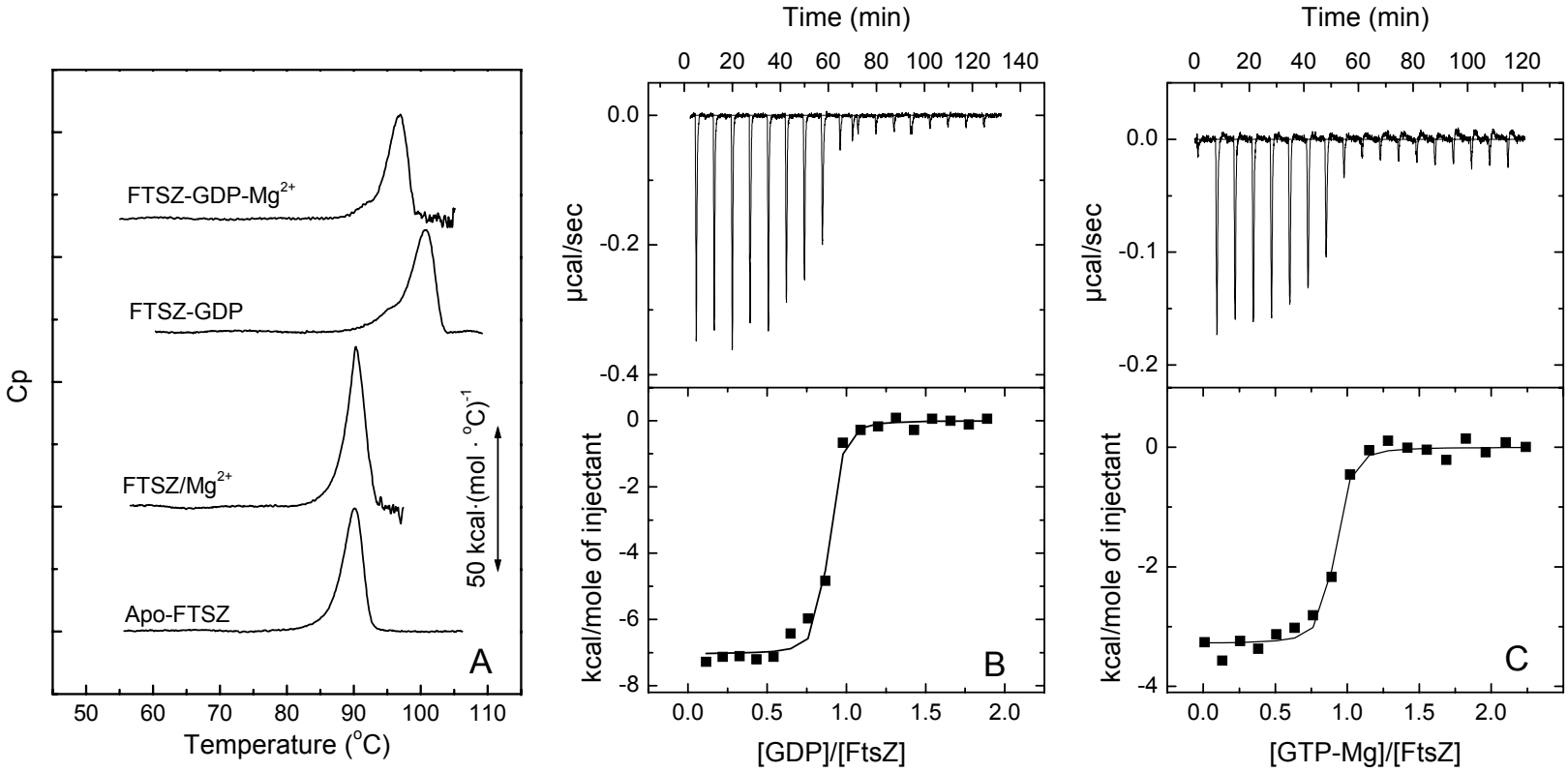

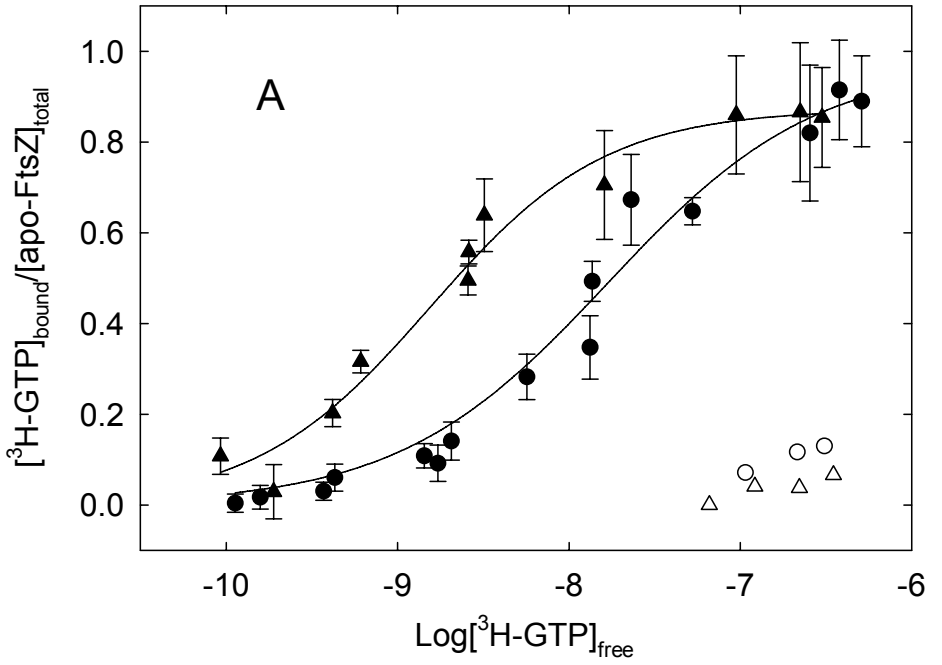

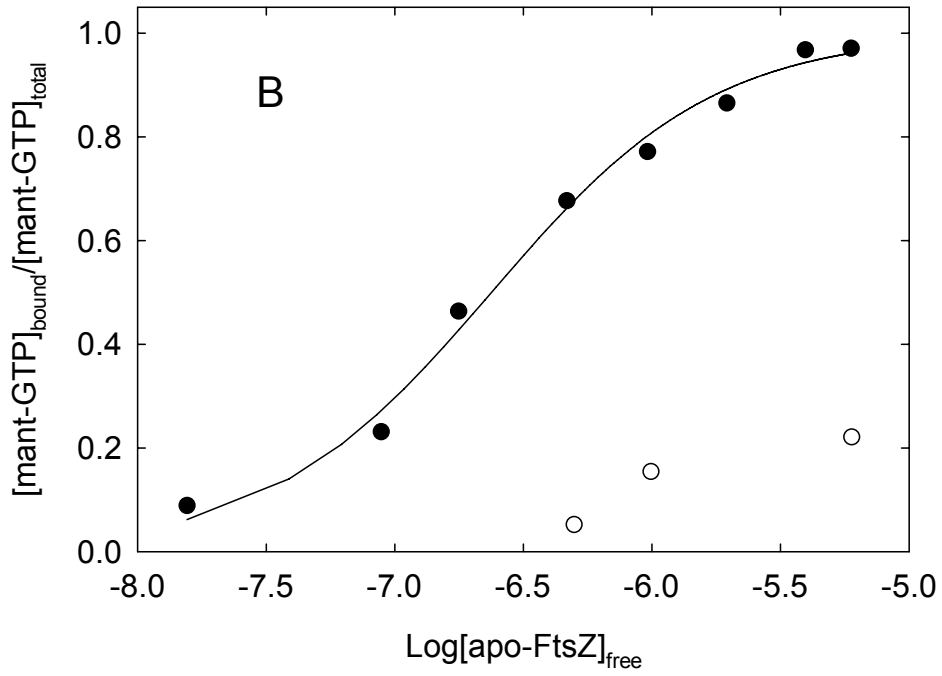

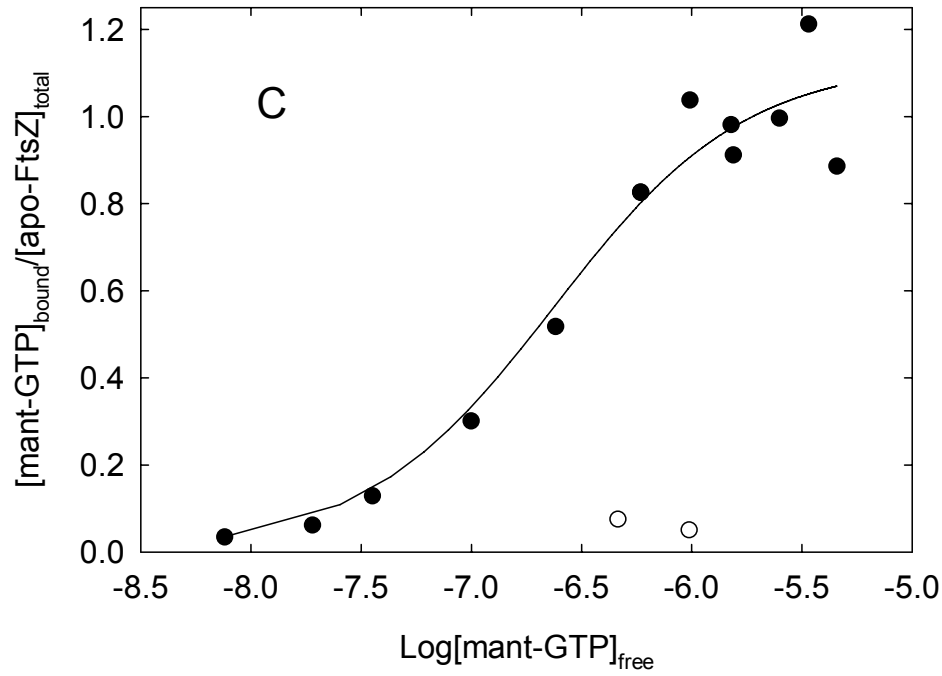

Figure 2

Figure 3

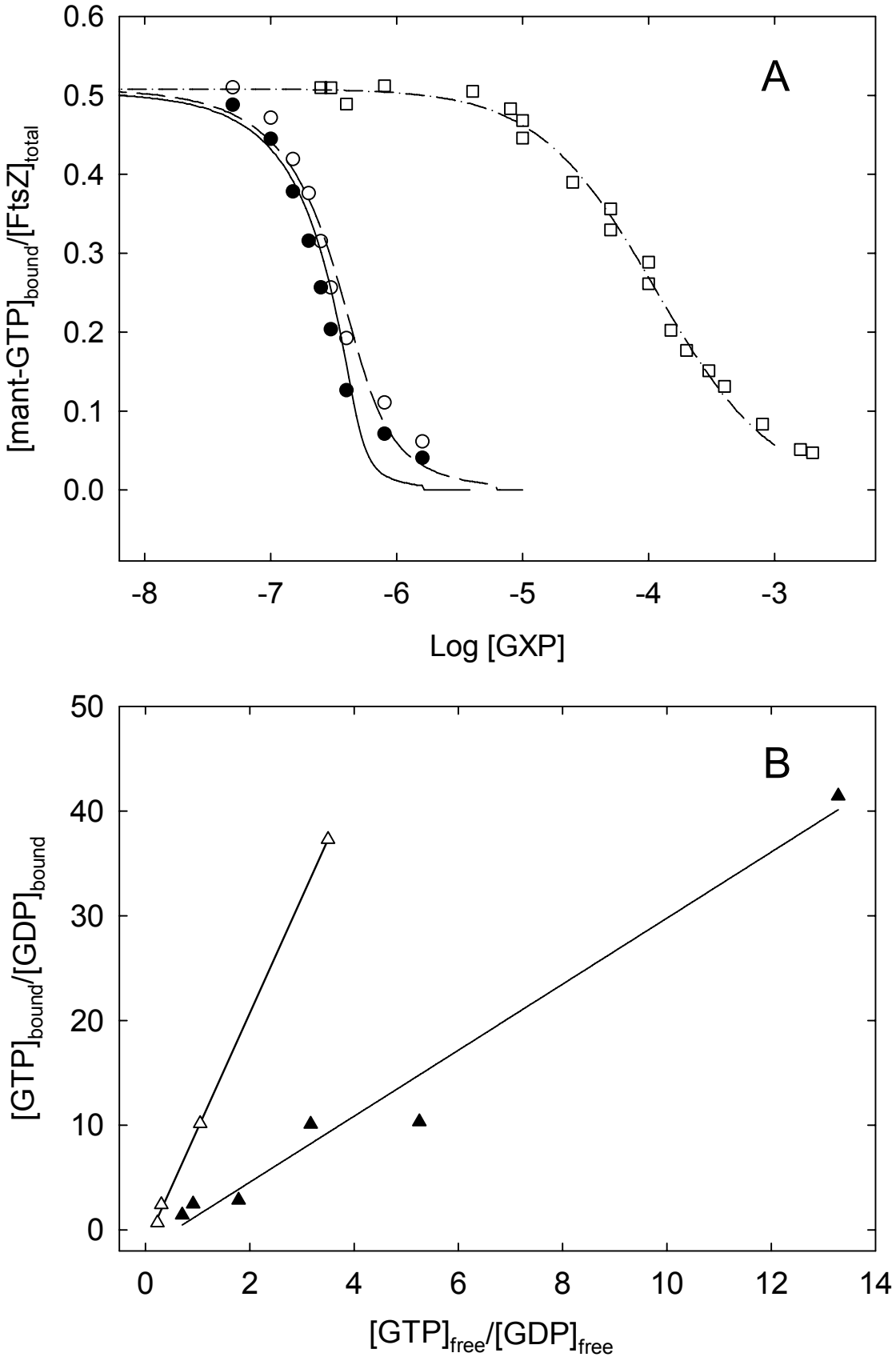

Figure 4

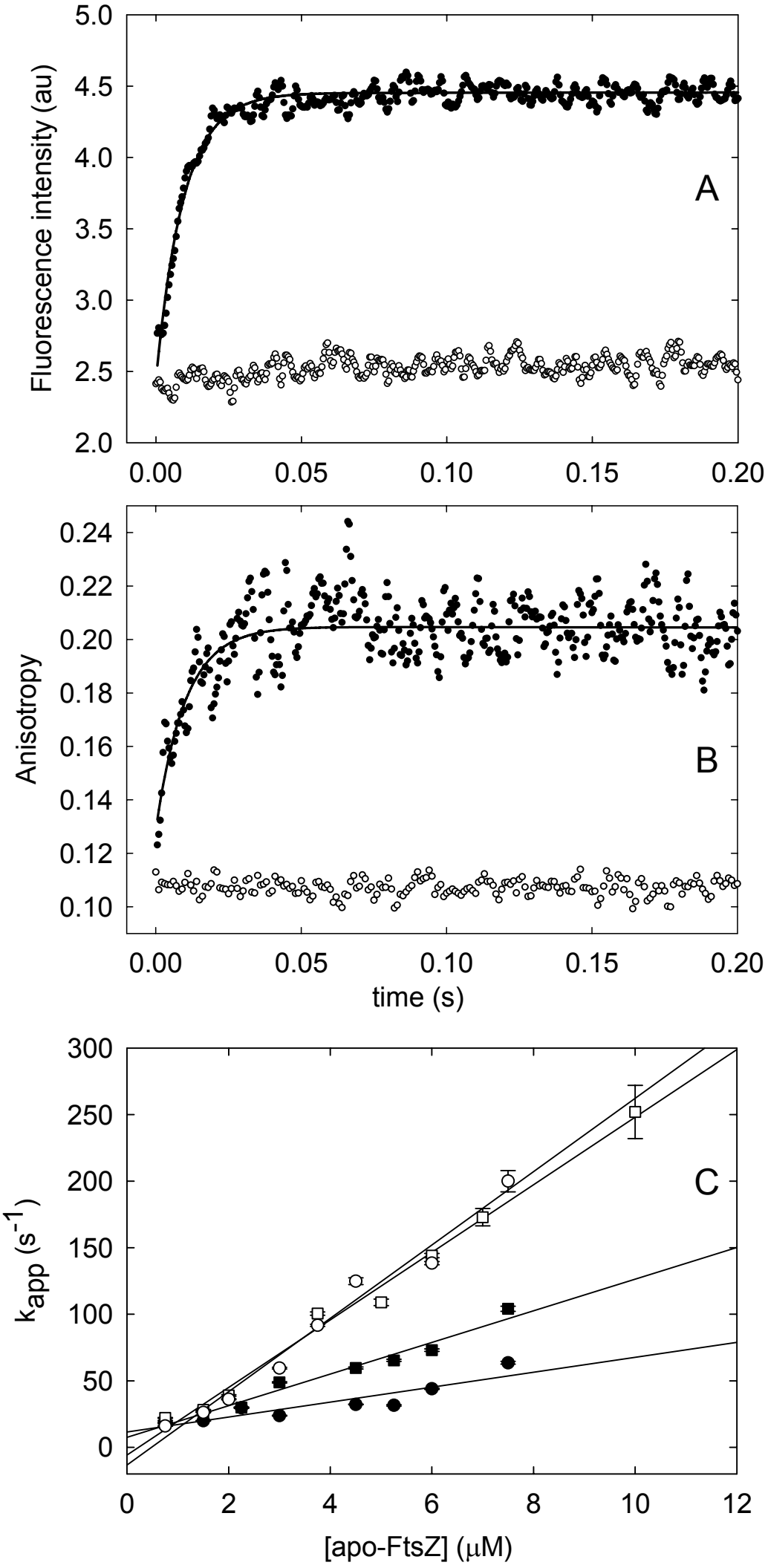

Figure 5

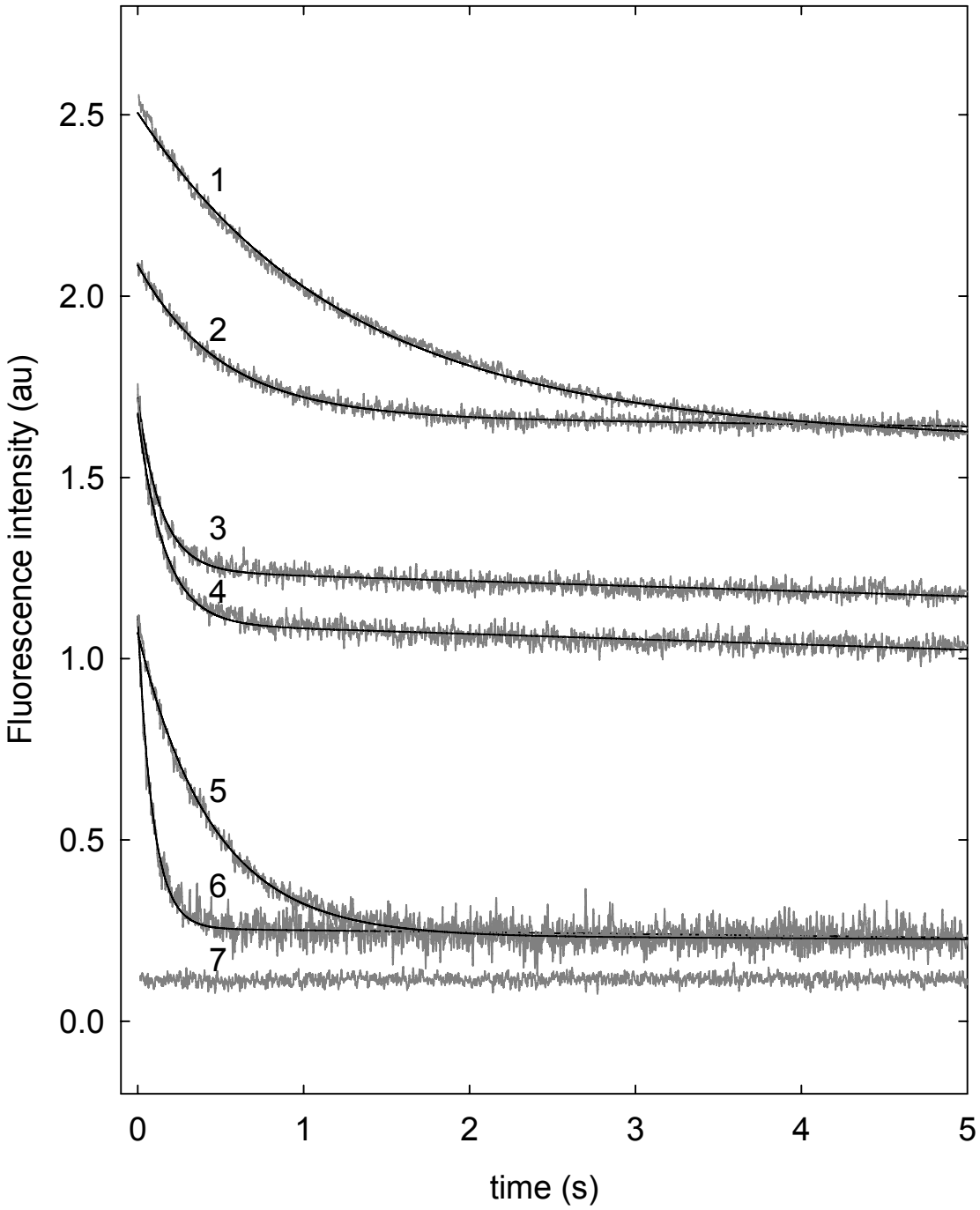

Figure 6

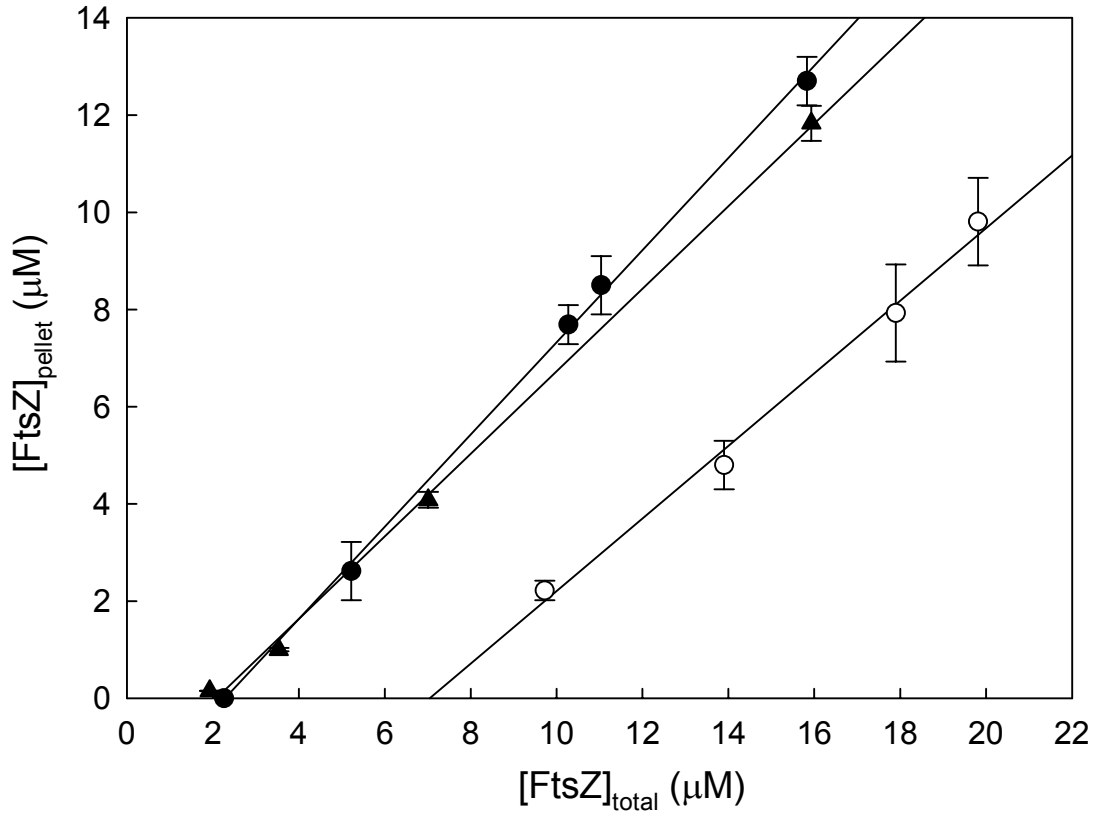

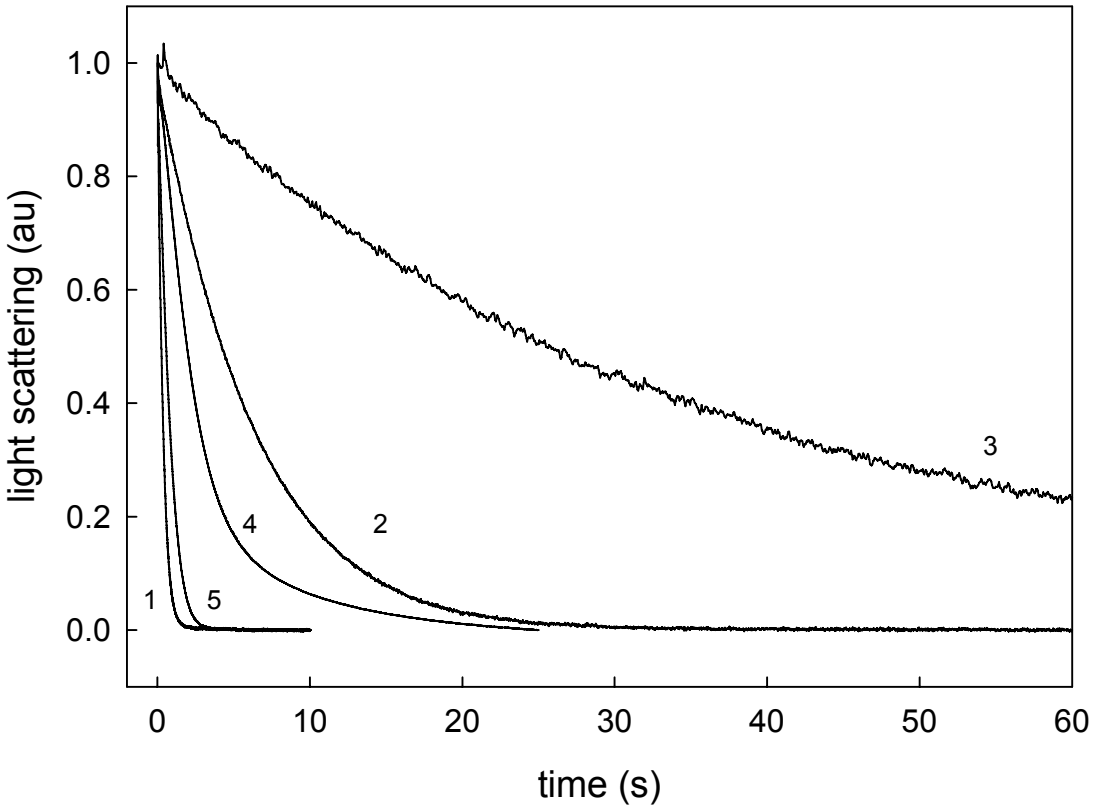

Figure 7

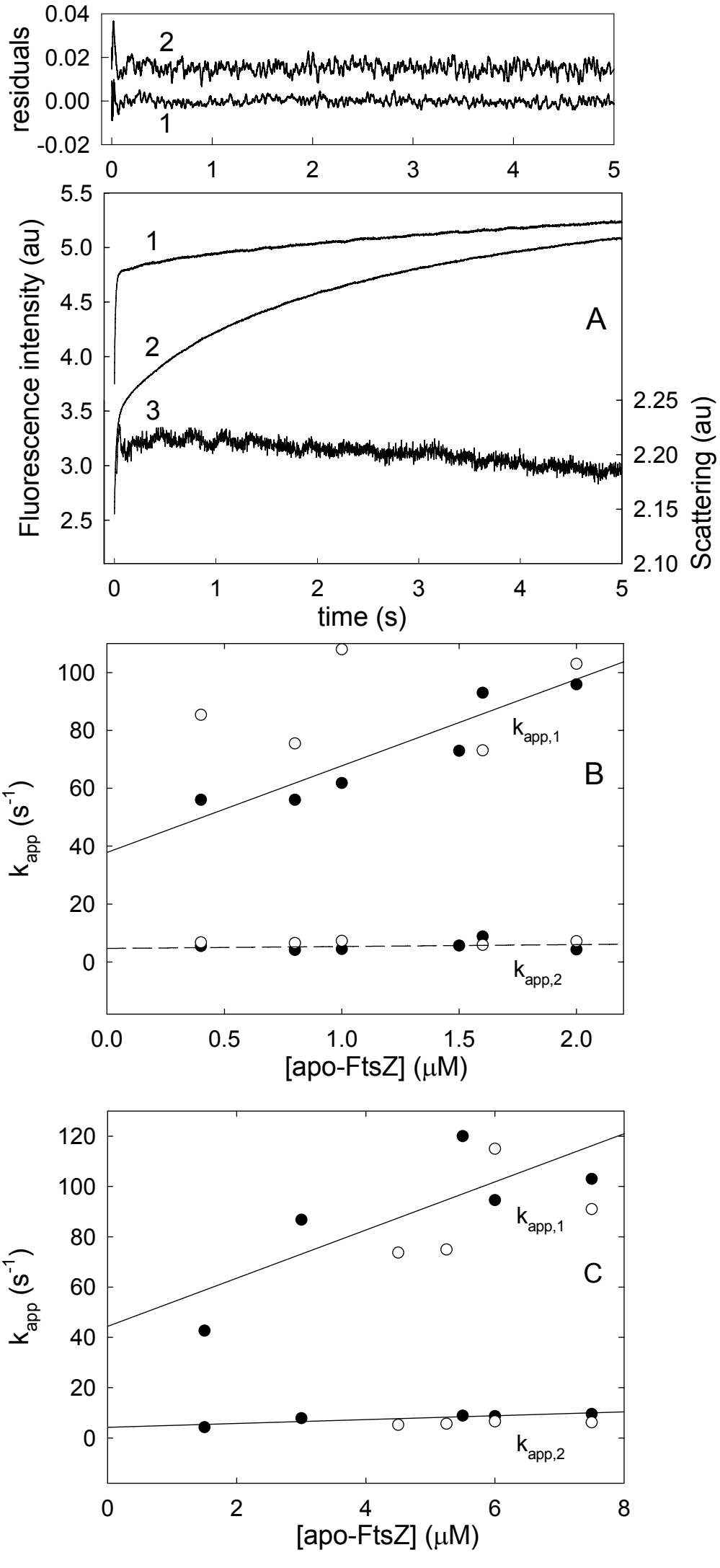

Figure 8

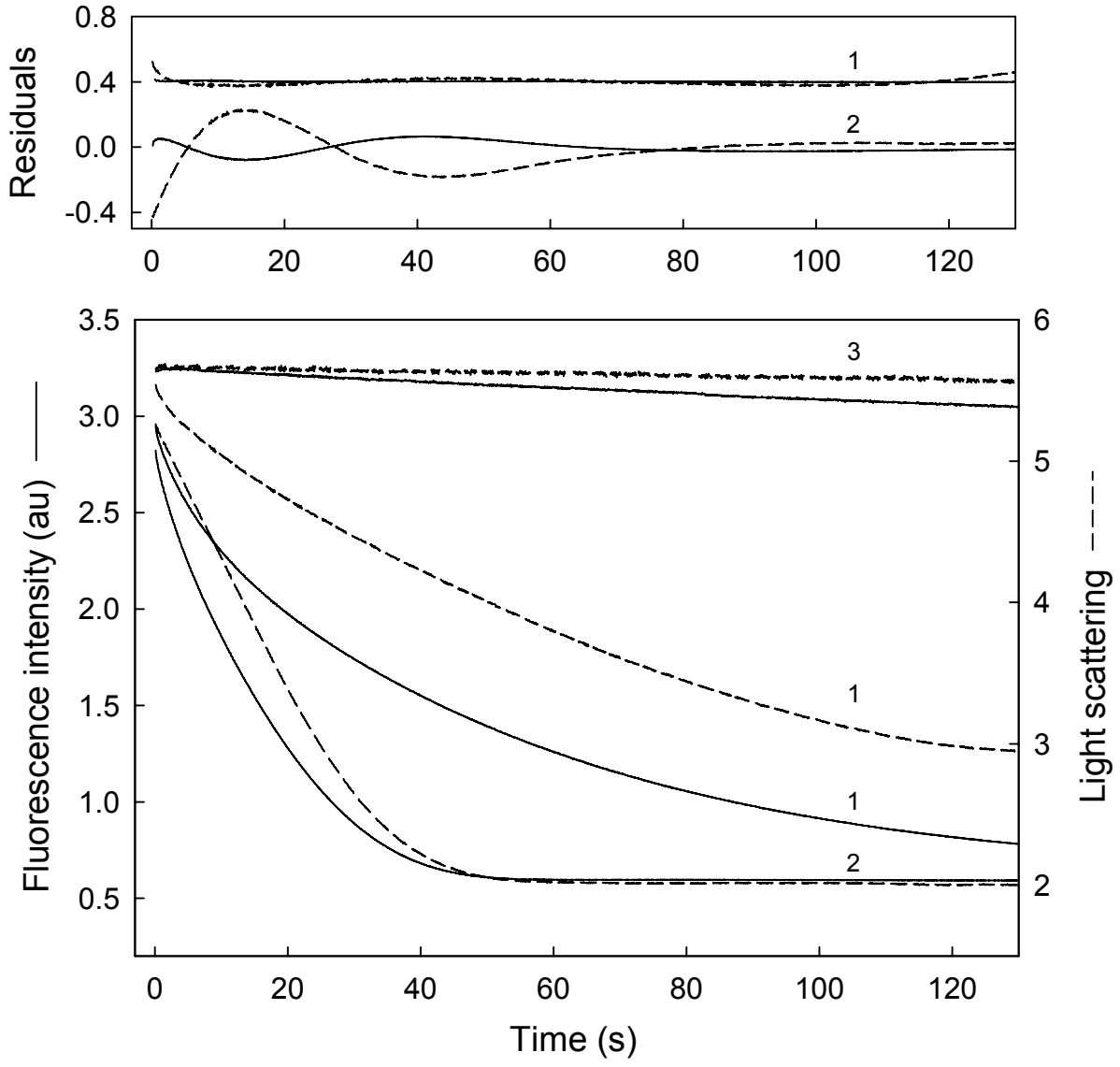

Figure 9

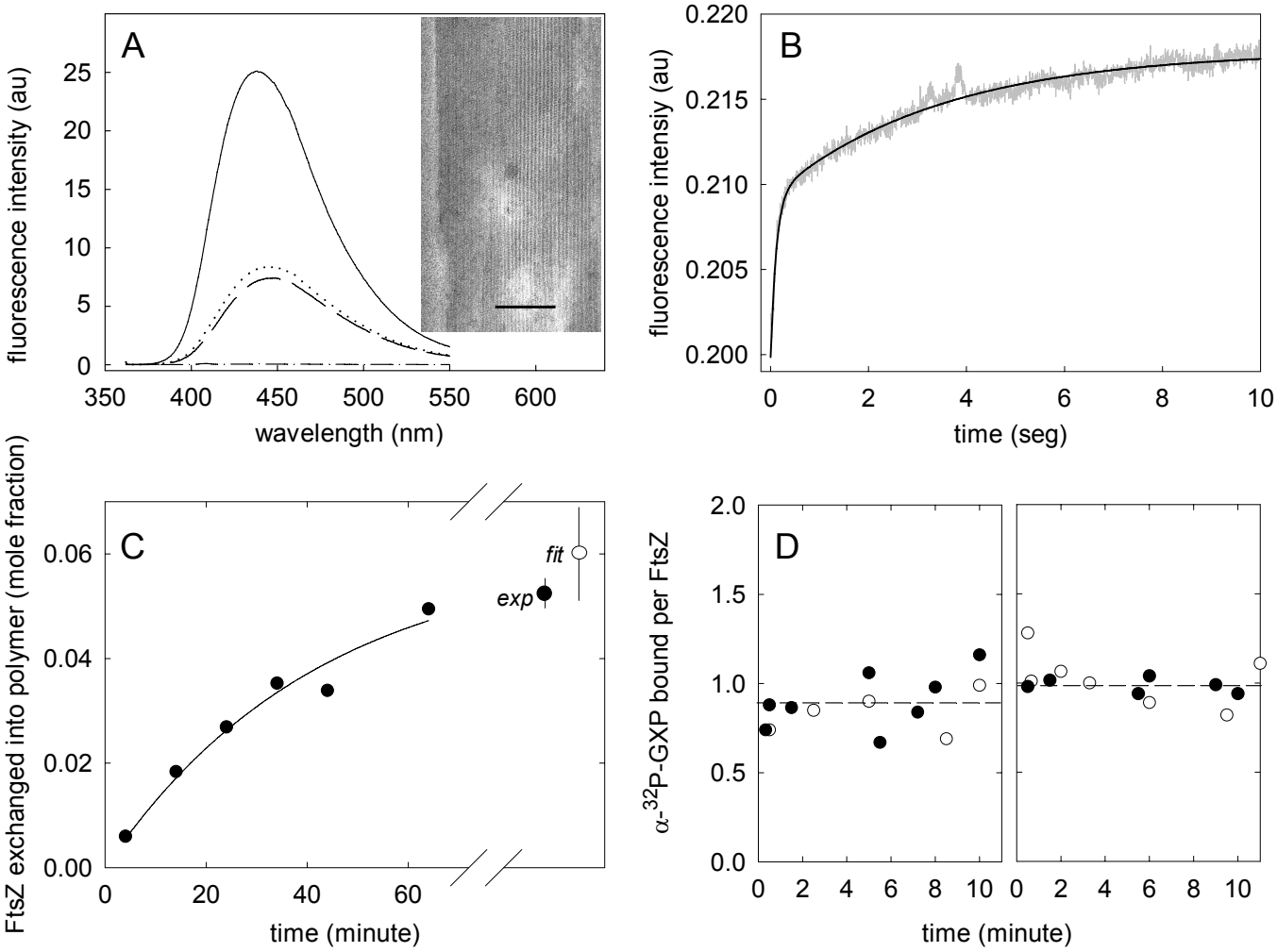

Figure 10